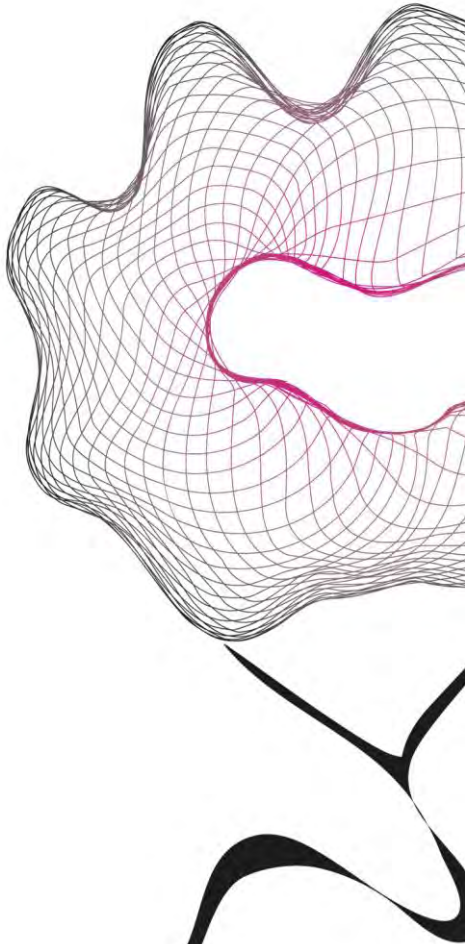


MASTER THESIS



NEEDLE AND SOFT-TISSUE SIMULANT INTERACTIONS: EXPERIMENTAL DESIGN AND OBSERVATIONS

Y.R.J. van Veen

FACULTY OF ENGINEERING TECHNOLOGY
LABORATORY OF BIOMECHANICAL ENGINEERING

EXAMINATION COMMITTEE
prof. dr. ir. Herman van der Kooij
dr. Sarthak Misra
ir. Edsko Hekman

DOCUMENT NUMBER
BW - 338

FACULTY OF ENGINEERING TECHNOLOGY

*Needle and Soft-Tissue Simulant Interactions:
Experimental Design and Observations*

Author:
Youri van Veen

Supervisors:
Prof. Dr. Ir. Herman van der Kooij
Dr. Sarthak Misra

June 14, 2011

Management Summary

Management Summary - English Version

Before you lies the graduation report of Youri van Veen, masterstudent mechanical engineering at the University of Twente. The graduation assignment, which is described in Chapter 1 of this report, consists of design and construction of a needle insertion device and performing experiments using this device. The needle insertion device will be used to do research on needle tissue interaction. The results from this research will be used in the MIRIAM project from the MIRA institute. MIRIAM stands for 'Minimally Invasive Robotics In An MRI environment'. A goal of this project is to build a robot which is capable of performing a prostate biopsy and brachytherapy. Brachytherapy is a form of radiotherapy to treat prostate cancer. For this robot models have to be created that describe the interaction between needle and tissue. These models will be implemented in the control structure of the robot. The beforementioned needle insertion device will be used to do research and help in the creation of needle tissue interaction models.

Chapter 2 of this report describes the design process of the needle insertion device. A problem analysis is performed from which a list of specifications and requirements is derived. With this list a number of concepts are considered. Among these concepts are a linear stage concept, a robotic arm concept, a friction based actuation concept and a linear motor concept. The linear stage concept is chosen and constructed. The chosen concept consists of a linear stage for translation of the needle. On top of the stage a rotary motor makes it possible to rotate the needle. Thus the concept is capable of inserting a needle with two degrees of freedom (one translational and one rotational) into a phantom. The concept is capable of recording forces and torques acting on the base of the needle via a force/torque sensor. Further, a charge coupled device (CCD) camera or an ultrasound device make it possible to record the insertion of the needle. After the construction phase the necessary software to actuate the device is created and the control structure is described. A proof of principle is performed to see whether the design performs according to the required accelerations and velocities. From the validation it is shown that a needle can be inserted with the required acceleration of 10 m/s^2 with a maximum insertion velocity of 300 mm/s . Rotation of the needle also performs according to the required specifications and is able to rotate a needle with a sinusoidal motion with a maximum angular velocity of 5 Hz and a maximum angular displacement of 180° .

Chapter 3 describes the research that is done with the needle insertion device. The results are written in journal paper form and will be sent to the *Medical Engineering and Physics* journal. The goal of this research is to determine the influence of six parameters on the needle-tissue interaction. The parameters include insertion velocity, needle diameter, needle bevel angle, needle tip shape, gel elasticity and motion profile. Experiments are performed with stainless steel rods on a gelatin phantom and observations are made by measuring the insertion force at the base of the needle and recording the insertion with a CCD camera. From the camera images the amount of needle deflection is obtained. Results show that with increasing insertion velocity, from $v = 5 \text{ mm/s}$ to 300 mm/s , that the insertion force increases to an asymptote of 6 N , while the maximum needle deflection decreases to an asymptote of 7.8 mm .

Increasing needle diameter from $\phi = 1 \text{ mm}$ to 2 mm results in increased insertion force while the amount of needle deflection decreases. These effects are due to an increased second moment of inertia of the needle.

Experiments on increasing the bevel angle, between $\beta = 8^\circ$ and 82° , show a nonlinear and increasing trend for insertion force and needle deflection. These results are explained with results obtained from experiments in which the microscopic effects at the needle tip are observed.

Four different needle tip shapes are tried to detect the influence of tip shapes on maximum insertion force and needle deflection. The tip shapes are a bevel tip, a franseen tip, a diamond tip and a conical tip. Results show that the asymmetrical bevel tip results in the highest amount of needle deflection when compared to the other shapes. The maximum insertion force however did not change significantly for all shapes.

Increasing the gel elasticity from $E_1 = 8.7$ kPa to $E_3 = 58.1$ kPa generally results in higher insertion force and needle deflection. There is one exception for the stiffest phantom ($E_3 = 58.1$ kPa) and the largest diameter needle ($\phi = 2$ mm). In that case a perpendicular crack occurs during insertion which results in less needle deflection.

Different motion profiles were also investigated. Results show that adding a 1 Hz sinusoidal rotation with an angular displacement of 180° to an insertion with a bevel needle, decreases the amount of needle deflection by $\sim 96\%$ but increases the insertion force by $\sim 12\%$ which could indicate more tissue damage. Increasing the angular velocity to 5 Hz decreases the insertion force which could indicate less tissue damage but research in this area is required. A tapping insertion does not result in significant changes in needle deflection but it does increase the insertion force.

Results from this research could be used in studies on navigating a needle through soft tissues. Knowledge on the deflection of the needle and force acting on the needle are required to plan a path through a tissue.

Chapter 4 concludes the report by presenting conclusions on the assignment and a list of recommendations. The recommendations are given with regard to adaptations for the device and topics and directions for future research.

Management Samenvatting - Nederlandse Versie

Het verslag wat voor U ligt betreft het afstudeerverslag van Youri van Veen, student werktuigbouwkunde aan de Universiteit Twente. De afstudeeropdracht welke beschreven staat in hoofdstuk 1 van dit verslag betreft het ontwerpen en construeren van een naald insertie apparaat. Tevens worden er met dit apparaat ook een aantal experimenten uitgevoerd. Het apparaat zal gebruikt worden om onderzoek te doen naar de interactie tussen naald en weefsel. De resultaten van dit onderzoek zullen gebruikt worden binnen het MIRIAM project van het MIRA instituut. MIRIAM staat voor 'Minimally Invasive Robotics In An MRI environment'. Een doel van dit project is om een robot te construeren die in staat is om een prostaat biopsie en een brachytherapie procedure uit te voeren. Brachytherapie is een vorm van radiotherapie om prostaat kanker te bestrijden. Voor deze robot moeten er modellen komen die de interactie tussen naald en weefsel beschrijven, deze modellen zullen dan worden geïmplementeerd in de aansturing van de robot. Het eerder genoemde naald insertie apparaat zal helpen in de ontwikkeling van deze naald-weefsel interactie modellen.

In hoofdstuk 2 van dit verslag wordt het ontwerp proces van het naald insertie apparaat beschreven. Er is een probleemanalyse uitgevoerd waaruit een lijst met eisen en specificaties is voortgekomen. Met deze lijst zijn een aantal concepten bedacht waaronder een spindelslede concept, een robotische arm concept, een wrijvingsgeactueerd concept en een lineaire motor concept. Uiteindelijk is het spindelslede concept gekozen en geconstrueerd. Het bestaat uit een spindel met slede voor translatie en op de slede is een motor gezet die in staat is om een naald te roteren. Het concept is dus in staat om een naald met twee vrijheidsgraden (een translatie en een rotatie) in een fantoom in te brengen. Het concept is verder in staat om kracht en torsie metingen te verrichten op de basis van de naald via een kracht en torsie sensor. Verder is het mogelijk om een charge-coupled-device (CCD) camera of een ultrasound apparaat aan te sluiten op het systeem welke het mogelijk maakt om de insertie van een naald op te nemen. Na de constructie van het apparaat is de software en de aansturingsstructuur gecreëerd om het apparaat aan te sturen. Tevens is een validatie uitgevoerd om te kijken of het apparaat voldeed aan de vereiste snelheden en acceleraties. Uit de validatie blijkt dat het apparaat volgens de eisen een naald kan inserteren met een versnelling van 10 m/s^2 en met een topsnelheid van 300 mm/s . De rotatie van de naald werkt ook volgens de specificaties en is in staat om een naald te roteren met een maximale hoeksnelheid van 5 Hz en met een maximale hoekverplaatsing van 180° .

In Hoofdstuk 3 is het onderzoek beschreven welke uitgevoerd is met het apparaat. Het doel van het onderzoek is om te kijken naar een zestal parameters en hun invloed op de interactie tussen naald en weefsel. De parameters die zijn bekeken betreffen, de insertie snelheid van de naald, de diameter van de naald, de bevel hoek van een bevel naald, de vorm van de naald tip, de stijfheid van een gelatine fantoom en het type beweging waarmee de naald wordt geïnserteerd in een fantoom. De resultaten zijn geschreven in de vorm van een journal paper en zullen gestuurd worden naar de *Medial Engineering and Physics* journal. De experimenten zijn uitgevoerd met draden gemaakt van roestvast staal welke dienst deden als naald. De inserties zijn uitgevoerd op een fantoom gemaakt van gelatine. De observaties bestaan uit insertiekracht metingen op de basis van de naald en hoeveelheid naald deflectie. De naald deflectie werd geëxtraheerd uit de opgenomen video beelden van de CCD camera. Er blijkt uit de resultaten dat het verhogen van de insertie snelheid van $v = 5 \text{ mm/s}$ tot en met 300 mm/s , ertoe leidt dat de maximale insertiekracht toeneemt naar een asymptoot van 6 N terwijl de naald deflectie afneemt naar een asymptoot van 7.8 mm .

Een toename van de naald diameter van $\phi = 1 \text{ mm}$ tot en met 2 mm heeft het effect dat de maximale insertiekracht toeneemt terwijl de hoeveelheid naald deflectie afneemt. Deze effecten komen door de toename van het oppervlaktetraagheidsmoment. Hierdoor neemt de resistentie tegen buiging toe.

Het verhogen van de bevel hoek van de naald, tussen $\beta = 8^\circ$ en 82° , laat een niet-lineaire toenemende trend zien voor de maximale insertiekracht en hoeveelheid naald deflectie. Er is een set met experimenten gedaan die kijkt naar de microscopische effecten die voorkomen bij de naald tip. De resultaten van deze experimenten geven een verklaring voor het niet-lineaire gedrag.

Vier verschillende naald tip vormen zijn geprobeerd om te kijken wat het effect hiervan kan zijn op de maximale insertiekracht en naald deflectie. De vier vormen zijn een bevel tip, een diamant tip, een franseen tip en een conische tip. Uit de resultaten blijkt dat de asymmetrische bevel tip de grootste deflectie levert. De maximale insertiekracht blijft relatief gelijk $\sim 2.8 \text{ N}$ voor alle tip vormen.

Toename van de fantoom stijfheid van $E_1 = 8.7 \text{ kPa}$ tot en met $E_3 = 58.1 \text{ kPa}$, resulteert in hogere

maximale insertiekrachten en naald deflectie. Er is een uitzondering voor het geval van de stijfste fantoom ($E_3 = 58.1$ kPa) en de dikste diameter ($\phi = 2$ mm). In dit geval ontstaat er tijdens de insertie een scheur in het fantoom loodrecht op de insertierichting welke ervoor zorgt dat er relaxatie optreedt. Deze relaxatie resulteert in een lagere hoeveelheid naald deflectie.

Als laatste zijn er een drietal bewegingsprofielen onderzocht. De resultaten laten zien dat het toevoegen van een rotatie met een hoek snelheid van 1 Hz en een hoek verplaatsing van 180° aan een insertie met een bevel tip naald, het effect heeft dat de hoeveelheid naald deflectie afneemt met 96% terwijl de maximale insertiekracht toeneemt met ongeveer 12%. Deze toename kan erop duiden dat er meer weefselschade optreedt. Als de hoeksnelheid wordt verhoogd naar 5 Hz dan blijkt dat de maximale insertiekracht afneemt wat erop kan duiden dat er minder weefselschade optreedt maar hier zal meer onderzoek naar gedaan moeten worden. Een tikkende insertiebeweging vergeleken met een continue insertie gaf geen significant verschil in de hoeveelheid naald deflectie maar er bleek wel dat de maximale insertiekracht toeneemt.

De resultaten van dit onderzoek kunnen gebruikt worden in onderzoeken op het gebied van het navigeren van een naald door een zacht weefsel. Kennis op het gebied van naald deflectie en insertiekrachten zijn nodig bij padplanning.

In hoofdstuk 4 worden er een aantal conclusies gepresenteerd omtrent de opdracht. Tevens worden er aanbevelingen gedaan met betrekking tot aanpassingen op het apparaat en richtingen en onderwerpen voor toekomstig onderzoek.

Preface

It has been 11 months since I started working on my graduation assignment to obtain my Master of Science degree. In these 11 months I have learned a lot and done much work of which I can be proud. I liked this project very much since it gave me the opportunity to design a device and build it myself from scratch. Besides that I also got the opportunity of performing experiments with my device and getting results out of it that are worth publishing in a scientific journal. At the end of this project there is a device which can perform needle insertions into soft tissue, but this would not have been possible without help from others. Therefore I would like to thank some people who helped me in one way or another. First of all Sarthak Misra for being my daily supervisor throughout the project. Although we not always saw everything on the same line, I believe that he helped me a lot in performing my work in a way that I did not think was possible for me. Second I would like to thank Herman van der Kooij for being my supervisor from the biomechanical engineering group. Third I would like to thank the technicians from the Control Engineering group for helping me out with so many things and/or components that I needed. Fourth I would like to thank all the new friends I made in the CE group. I like the coffee breaks and lunches we had but especially the humorous discussions we had during these breaks. I hope you guys also graduate soon. Last but not least I would like to thank my girlfriend Gonneke for just being there whenever I stressed out too much and for getting me back on track. I leave you now and hope that you will get some useful information out of this report which I have spent so much time on.

Youri van Veen
June 14, 2011

List of Figures

1.1	DynaTRIM	1
1.2	Anatomy overview of the location of a prostate.	2
2.1	The total design of the Needle Insertion Device	7
2.2	The design of the Linear Stage	7
2.3	A topview and sideview of the Linear Stage	8
2.4	Manual slide table	10
2.5	The constructed needle insertion device	11
2.6	Control Structure NID	12
2.7	Position and velocity profile of translation with a velocity of 300 mm/s	14
2.8	Sinusoidal motion profile with a frequency of 1 Hz and an angular displacement of $\pm 90^\circ$.	14
2.9	Sinusoidal motion profile with a frequency of 5 Hz and an angular displacement of $\pm 90^\circ$.	15
2.10	Sinusoidal motion profile with a frequency of 5 Hz and an angular displacement of $\pm 90^\circ$.	15
3.1	Two DOF needle insertion setup used for macroscopic experiments	20
3.2	Four different needle tip shapes	20
3.3	Experiment setup for microscopic experiments	21
3.4	Maximum insertion force and needle deflection with varying insertion velocities	23
3.5	Maximum insertion force and needle deflection with varying needle diameter and gel elasticity	23
3.6	Insertion force versus time of a needle insertion into a gelatin phantom	24
3.7	Maximum insertion force and needle deflection with varying bevel angle	24
3.8	Maximum insertion force and needle deflection with varying needle tip shape	25
3.9	Maximum insertion force and needle deflection with varying motion profile - rotation . . .	25
3.10	Maximum insertion force and needle deflection with varying motion profile - tapping . . .	26
3.11	Tip crack for various bevel angles	27
3.12	Compression of the gel for various bevel angles	28
3.13	Forces and torques versus insertion distance for a needle insertion in a gelatin phantom .	28
3.14	$ F_z $ and $ T_y $ versus insertion distance for needles with $\beta = 30^\circ$, $\beta = 60^\circ$ and $\beta = 75^\circ$. . .	28
3.15	$ F_z $ and $ T_y $ versus insertion distance for $\phi = 1$ mm and $\phi = 1.6$ mm	29
3.16	$ F_z $ and $ T_y $ versus insertion distance for different gel elasticities	29
A.1	IPM of the motor, gearhead, spindle and load	41
A.2	Velocity profile	42
A.3	Free Body Diagram of the Load	43
A.4	Free Body Diagram Spindle + Gearhead	43
A.5	Free Body Diagram Motor	45
A.6	Ideal Physical Model of rotation of the needle	46
A.7	Position profile - frequency 5 Hz - angular displacement 90 degrees	46
A.8	Free Body Diagram Motor Needle Rotation	47
B.1	Linear Motor concept	49
B.2	Robotic arm concept	50

B.3 Friction drive concept 51

List of Tables

2.1	Motion profiles for Proof-of-Principle	13
3.1	Macroscopic Experiment Plan	20
3.2	Elasticity values of gelatin phantoms in kPa.	20
A.1	Parameters	41
A.2	Motion profile time parameters	42
A.3	Parameters	43
A.4	Parameters of Maxon Gearhead GP26B	44
A.5	Parameters	45
A.6	Maxon RE25 motor parameters	45
A.7	Calculation Parameters	47
A.8	Maxon ECTMax22 motor parameters	48

Contents

Preface	vii
List of Figures	ix
List of Tables	xi
Table of Contents	xiii
1 Introduction	1
2 Design and Construction of a Needle Insertion Device	5
2.1 Introduction	5
2.2 Problem analysis	5
2.3 Specifications and requirements	6
2.3.1 Mandatory requirements	6
2.3.2 Wishes	6
2.4 Design of the NID	7
2.4.1 Linear stage	7
2.4.2 Manual slide table	10
2.5 Construction of the NID	11
2.5.1 Control and actuation of the NID	11
2.5.2 Sinusoidal motion generation	12
2.5.3 Proof of principle	13
2.5.4 Conclusion	16
3 Macroscopic Observations of Needle-Tissue Insertions	17
3.1 Abstract	18
3.2 Introduction	18
3.3 Experimental Setup	19
3.3.1 Macroscopic Study	19
3.3.2 Microscopic Study	21
3.4 Observations and Results	22
3.4.1 Macroscopic Observations of Needle-Tissue Interactions	22
3.4.2 Microscopic Observations of Needle-Gelatin Phantom Interactions	27
3.5 Conclusion and Future Work	30
4 Conclusions and Recommendations	31
4.1 Conclusions	31
4.2 Recommendations	32
4.2.1 Needle Insertion Device	32
4.2.2 Future research	33
References	35

Appendices	39
A Motor Calculations	41
B Design Concepts	49
B.1 Linear motor	49
B.2 Robotic arm	50
B.3 Friction drive concept	50

Chapter 1

Introduction

Yearly around 1.5 million people from the US and 83,000 people from the Netherlands are diagnosed with a form of cancer [12, 32]. Cancer is a group of diseases characterized by an uncontrolled cell growth. If the growth and spread of cells is not contained it can result in death. One specific type of cancer is prostate cancer and it is diagnosed in around 200,000 men in the US and 10,000 men from the Netherlands every year. This makes prostate cancer the most common cancer, apart from skin cancer. From these cases an estimated 30,000 men from the US and 3000 men from the Netherlands eventually die because of this disease. The symptoms of prostate cancer can include frequent urination especially at night, difficulty starting urination and maintaining steady flow, painful urination, impotence and others.

Diagnosis To determine whether a patient is afflicted with this disease and what kind of cancer it is, a biopsy of the prostate can be taken. One type of prostate biopsy incorporates the capabilities of a Magnetic Resonance Imaging scanner to correctly position the biopsy needle in the prostate gland. In case of this type of prostate biopsy, a needle guide as encircled in Figure 1.1 is inserted in the anus of the patient and positioned against the wall of the rectum. See Figure 1.2 for a overview of the location of a prostate inside the human body. A biopsy needle is then inserted in the guide and through the rectal wall into the prostate gland. Correct positioning of the needle tip is done manually with visual help from MR images. This method is time consuming and costly, since the physician has to manually position the needle, take a few MR images, reposition the needle based on the MR images and so on until it is correctly positioned and a biopsy can be taken. It is also very uncomfortable for the patient who has to lie inside the small bore (diameter ≈ 70 cm [31]) of a MRI scanner for up to an hour.



Figure 1.1: DynaTRIM (Invivo, Gainesville USA). A device which helps in the prostate biopsy procedure. The needle guide is encircled.

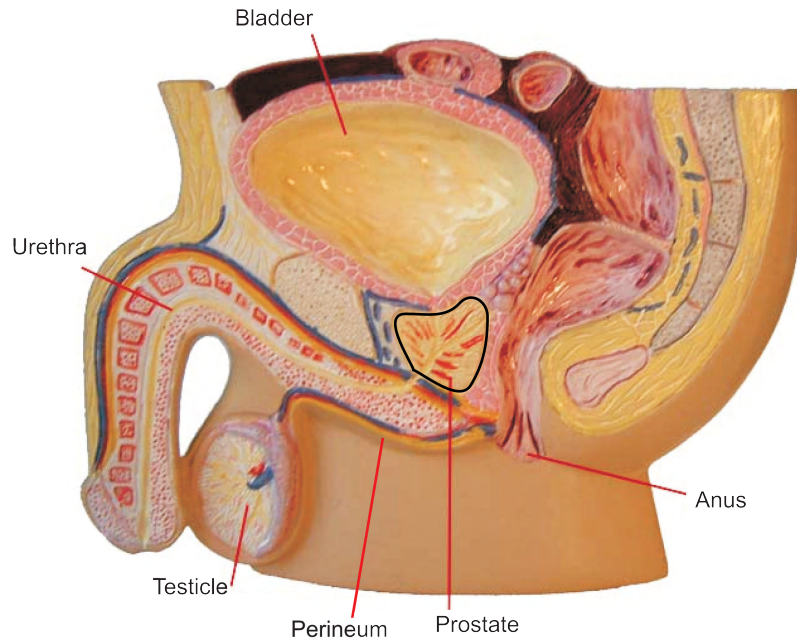


Figure 1.2: Anatomy overview of the location of a prostate.

Treatment When the diagnosis of prostate cancer is made it can be treated with a procedure called brachytherapy. Brachytherapy is a form of radiotherapy where a radioactive source is placed inside or near cancerous tissue. In case of a prostate brachytherapy procedure, multiple needles are inserted through the perineum and into the prostate. Each needle is inserted with a specific depth according to the location of the cancerous tissue. A radioactive seed is then inserted through the needle into the prostate. Correct positioning of these needles can be achieved with visual feedback from UltraSound images or MR images of the prostate and manually inserting the needles. This procedure is time consuming and costly, since a great number of needles and seeds have to be inserted and correctly positioned (≈ 18 needles and 55 seeds per treatment [33]).

Improving the Treatment In the medical world a needle insertion is a common minimally invasive procedure. It is used for numerous procedures including blood sampling, regional anesthesia, local drug delivery and tissue biopsies. One of the benefits of a minimally invasive procedure is the decrease of time that a patient is staying in the hospital to recuperate when compared to an operation where an incision is made. This means that more beds are available for other patients and that the cost of treating an affliction like prostate cancer is reduced. However there are still ways of improving the entire process. One aspect is the level of comfort for the patient who has to lie within a MRI scanner for up to an hour. Another aspect is reducing the amount of time it takes for a biopsy to be taken and the brachytherapy to be performed. Reducing the procedure duration also decreases the costs which is an important factor. One method of increasing the level of comfort for the patient and decreasing the costs of these procedures is that the needle insertion can be done using a, presumably faster, robotic needle insertion device.

A project named MIRIAM was started. MIRIAM stands for Minimally Invasive Robotics In an MRI-environment. The MIRIAM project is co-ordinated by the Control Engineering group at the University of Twente and the principal investigator is Dr. Sarthak Misra. This project has the goal, among others, to develop a robot which can perform a prostate biopsy and, or brachytherapy in an MRI environment. In order to develop this medical robot, research has to be done on needle insertions. Among many research subjects are the targeting accuracy of the needle, modeling of the needle-tissue interaction and methods of navigating a needle around obstacles. The project is relatively new and in order to start research on

needle insertions a needle insertion device has to be designed and built. This part of the project was made into a graduation assignment.

The Assignment The graduation assignment is divided in two major parts. The first part consists of designing and construction of a two degrees of freedom needle insertion device. This device can be used in a number of different experiments all looking at different aspects of needle-tissue interactions. The second part consists of a set of experiments with the intent on discovering how certain parameters influence the targeting accuracy of a needle during an insertion.

The setup of this master thesis is the following. In Chapter 2 the design process of the needle insertion device is described and the chosen concept is presented in detail. A proof of principle is given to show that the device is working according to the specifications. Chapter 3 describes the experiments that were performed to ascertain the influence of different parameters during needle insertion on targeting accuracy. The results of the experiments are written in the form of a journal paper. Chapter 4 concludes this thesis by presenting conclusions and a list of recommendations on adaptations on the needle insertion device and future research work. Appendix A lists the calculations that were done to determine which motors would be implemented in the device. Appendix B describes three design concepts that were not chosen to be built.

Chapter 2

Design and Construction of a Needle Insertion Device

2.1 Introduction

This chapter describes the design of the Needle Insertion Device (NID). First a problem analysis is performed from which a set of specifications and requirements is derived. After this the chosen concept of the needle insertion device is presented in detail. The chapter concludes with a proof-of-principle describing the performance of the design as it was built.

2.2 Problem analysis

The main function of the Needle Insertion Device will be to insert a needle into a phantom. The NID will have two Degrees Of Freedom (DOF) in which it can insert the needle. One translational DOF and one rotational DOF, in other words the needle can be inserted along the longitudinal axis of the needle and rotated about this axis.

The NID will act as a test bed for different experiments with different requirements. Therefore the device should be designed in such a way that many types of experiments can be done without having to redesign and/or rebuild the entire setup. This can be done by designing the setup in modules which can be detached from one another and quickly interchanged. For example one person may want to do experiments where an ultrasound imaging device will be used while another wants to use a Charge-Coupled Device camera. There should be an option of quickly changing from CCD camera to a setup with an ultrasound imaging device. Another aspect is that of the type and size of the phantom to be used. One phantom may be a small transparent object while another could be big and non-transparent.

In a number of experiments a block of gel will be used as a phantom in which a needle will be inserted. It is desired to be able to use one phantom for multiple insertions in order to save time so a mechanism to reposition the phantom or the needle needs to be incorporated. Otherwise only one needle insertion experiment can be performed and then another phantom has to be made.

In order to say something useful on the needle-tissue interaction it needs to be tracked or measurements are to be taken. This tracking can be done via visual feedback (e.g. camera, ultrasound or MR images) or non visual feedback (e.g. force/torque sensors, Fiber Bragg Grating sensors or pressure sensors). At least one of these methods need to be incorporated in the design but preferably more.

One type of research looks at flexible needles and methods of steering these needles around obstacles inside a phantom and reaching a certain target. These flexible needles will buckle when inserted without guidance and so a method should be incorporated to prevent buckling.

The insertion depth of the needle must be such that a prostate biopsy or brachytherapy can be simulated. According to Abolhassani et al. [2] there is a 7-10 cm layer of skin, muscle and fatty tissue that needs to be punctured in order to reach the prostate. This means that the insertion depth must be at least 10 cm.

Some research has been done on high insertion velocity needle insertions by Podder et al. [28] and Lagerburg et al. [16]. They inserted a needle with a maximum velocity of 200 mm/s and 31 m/s, respectively. Lagerburg showed that high velocity insertion decreases the amount of prostate motion which would increase targeting accuracy. For the NID it is desired to be able to perform high insertion velocity experiments. The rotational velocity was an experimental parameter in experiments performed by Podder et al. [28] They reached velocities of 300 rpm. It is desired to be able to reach the same high velocity.

Some research has been done in the area of variable acceleration during a needle insertion by Abolhassani et al. [2]. However they tried only low accelerations ($\leq 10 \text{ mm/s}^2$). Mahvash et al. [17] however tried an acceleration of 10 m/s^2 . In the interest of having the possibility of changing the acceleration in future experiments it is desired that the NID can insert a needle with an acceleration of 10 m/s^2 .

In regular prostate biopsy and brachytherapy a 17 Ga needle is typically used which equals a needle outer diameter of 1.4 mm. For a biopsy of a breast tumor the size can go up to a 14 Ga which equals a diameter of 2.1 mm. The needle insertion device should be able to work with the same diameters to be used as a testbed.

2.3 Specifications and requirements

The main purpose of the needle insertion device is to be able to insert a needle into a phantom. But to be more specific a list of specifications and requirements has been made to which the design should comply. These specifications and requirements are divided into two categories being, mandatory requirements and wishes. The design should comply with the first and it is preferred that it also complies with the second but this is not mandatory.

2.3.1 Mandatory requirements

- The NID has to be able to insert a needle into a phantom with two degrees of freedom. Translation in one direction and rotation about the translational axis.
- The needle is inserted into a phantom of varying size but within a size of $200 \times 200 \times 40 \text{ mm}$.
- The insertion velocity of the needle can be varied between: $1 - 300 \text{ mm/s}$.
- The insertion depth can be varied between: $0 - 150 \text{ mm}$.
- Acceleration of the needle: 10 m/s^2
- Rotation - minimum angular displacement of the needle: 180°
- Rotation - maximum velocity of the needle: 300 rpm
- Needle - attachable diameters: $0.3 - 3 \text{ mm}$
- Needle - attachable lengths: maximum 180 mm
- There should at least be one visual and one non-visual method of measurement applied to the needle. This could for example be a force/torque sensor combined with a camera
- The NID should be as compact as possible but within dimensions of $1200 \times 750 \times 300 \text{ mm}$. These are the dimensions of the optical table that the design will be attached to.

2.3.2 Wishes

- The NID should be designed as a modular device. In this way changes can be made to the setup fairly quickly and different experiments can easily be conducted.
- There should be an easy way of repositioning the phantom or needle in order to do multiple needle insertions in one phantom.
- A method to prevent buckling of flexible needles is desired in the design.

2.4 Design of the NID

With the list of specifications and requirements a number of concepts were considered. Among the concepts are a linear stage concept, a linear motor concept, a friction drive concept and a robotic arm concept. After careful consideration of many aspects the linear stage concept was chosen as the device which would be build. The other concepts are mentioned along with the arguments why these were not chosen in Appendix B. In Figure 2.1 the chosen design is shown.

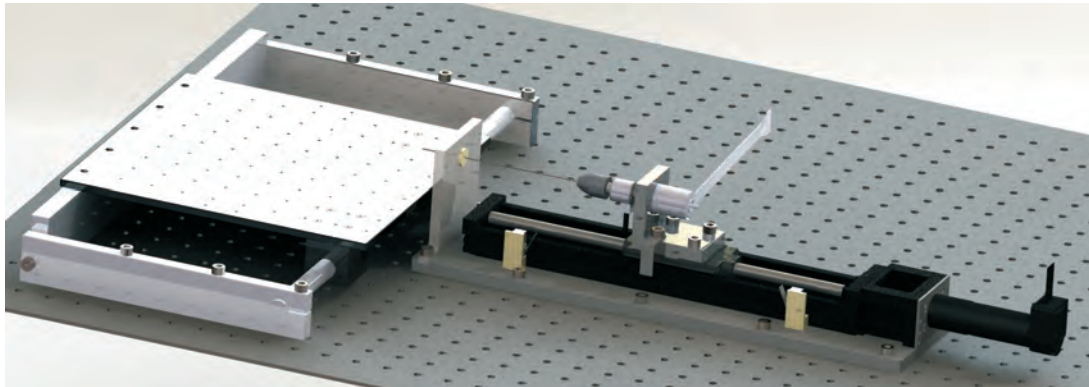


Figure 2.1: The total design of the Needle Insertion Device

The design consists of two major parts. The first being a section which performs the motion of the needle and houses all attributes needed to guide the needle. The second part consists of a sliding table which permits the translational motion of a phantom. Besides these two major parts there are also two Sony (Sony Corporation, Tokyo, Japan) XCD-SX90 Charge-Coupled Device cameras mounted over the sliding table which can record the needle during insertion. These cameras can also be interchanged for an ultra sound imaging device. Finally there are also two Elmo Whistle 2.5/60 controllers (Elmo Motion Control Ltd, Petach-Tikva, Israel) which are used to actuate and control the two motors implemented in the design.

2.4.1 Linear stage

In Figure 2.2 and 2.3 a closeup of the linear stage is shown. The following parts are implemented with the linear stage and are numbered in Figure 2.3.

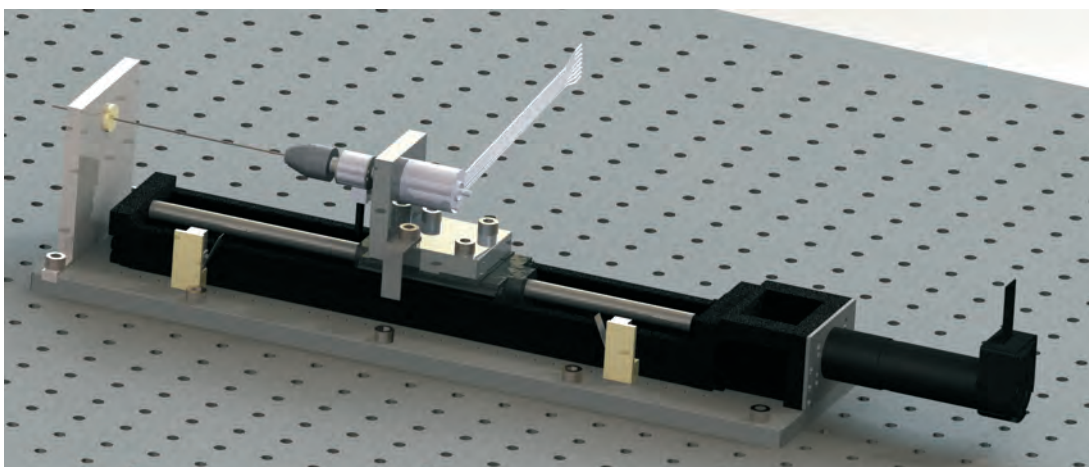


Figure 2.2: The design of the Linear Stage

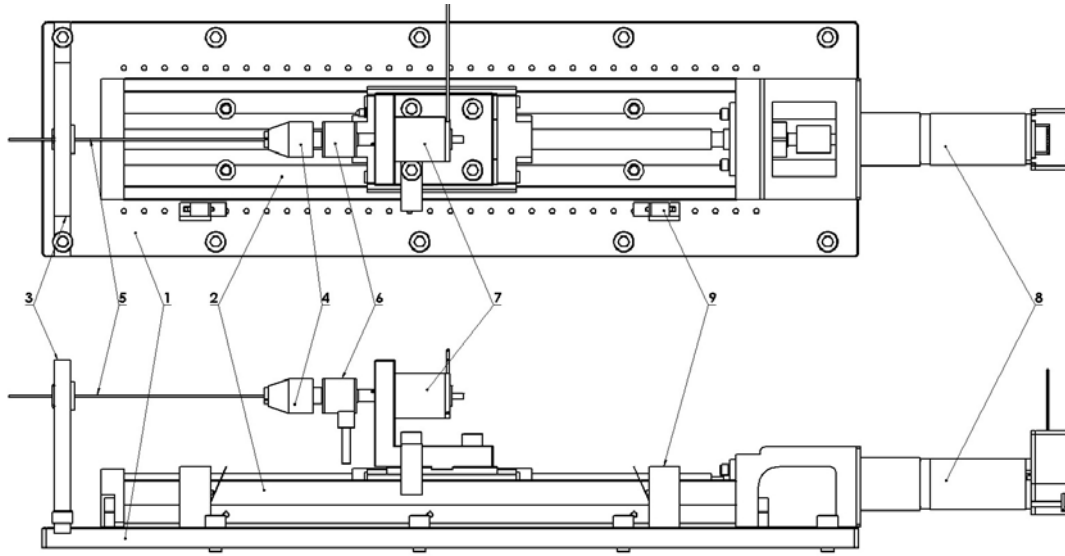


Figure 2.3: A topview and sideview of the Linear Stage

1. Aluminum Base Plate

This is the base plate, it serves as a foundation to which all the other parts connect to. It can be connected to an optical table via eight M6 bolts.

2. Linear Stage

A Misumi LX3010 linear stage(MISUMI Group Inc. Tokyo, Japan) makes translation of the needle possible. The linear stage is connected to the baseplate via two dowel pins and six bolts. The spindle of the stage has a length of 300 mm with a thread of 10 mm per revolution. The maximum stroke of the carriage equals 204 mm.

3. Needle guidance block and plug

The guidance block and plug were made to prevent buckling of flexible needles during insertion. The plug guides the needle and increases the buckling load (Eq. 2.1 in which F_{cr} : critical buckling load, E : modulus of elasticity, I : second moment of inertia, K : column effective length factor, L : length of column) since the column effective length factor K changes from $K = 2$ (no guidance plug) to $K = 1$ (Including guidance plug). Regarding the experimental results in Chapter 3 it is noted that stiff needles were used and the plug was removed in these experiments.

$$F_{cr} = \frac{\pi^2 EI}{(KL)^2} \quad (2.1)$$

4. Multichuck

A Proxxon multichuck (Proxxon GmbH, Niersbach, Germany) is used to attach needles to the NID. Needles with a diameter between 0.3 and 3.2 mm can be attached to the chuck.

5. Needle

The needle can be any diameter between 0.3 and 3.2 mm and the length may vary between 20 and 180 mm.

6. Maxon ECMax22 motor (Maxon Motor, Sachseln, Switzerland)

The Maxon ECmax22 motor is attached via an L-shaped aluminum block to the linear stage carriage and rotates the needle. The motor axis is directly connected to the force/torque sensor and needle without a gearhead. For the motor calculations see Appendix A and for detailed information regarding this motor see Table A.8.

7. Maxon RE25 motor

The Maxon RE25 motor actuates the linear stage. It consists of a 20 Watt RE25 motor with GP26B gearhead and a HEDL5540 encoder. The gearhead has a transmission ratio of 4.4:1 and the encoder has 500 pulses per revolution. For the motor calculations see Appendix A and for detailed information regarding this motor see Table A.6.

8. ATI Nano17 Force/Torque sensor (ATI Industrial Automation, Apex, USA)

A Nano17 Force/Torque sensor is mounted between the multichuck and the maxon ECTMax22 motor. This force/torque sensor has a force resolution of 3.125 mN and a torque resolution of 15.625 mNmm and is capable of measuring the small forces and torques that act on a needle during insertion.

9. Limit switch

Two limit switches are implemented for safety reasons. If the stage reaches this limit then both motors are shutdown. The switches can be mounted anywhere along the side of the stage to adapt the maximum travel distance for every different experiment.

2.4.2 Manual slide table

The manual slide table is shown in Figure 2.4. The purpose of this table is to mount a variety of phantoms on it and be able to translate it in one DOF perpendicular to the insertion direction. It was found that repositioning a block of soft tissue simulant like gelatin without changing the boundary conditions is relatively difficult. Repositioning a block of gelatin could result in rupture of the block or pieces breaking off. Failure of the gelatin phantom would result in the incapability of performing experiments and creating another gelatin phantom is time consuming. To solve this problem it was decided that the phantom would be positioned on a table which can then be repositioned by sliding the table.

The table itself is designed as a breadboard with M3 threaded holes so different dimensions of phantom material can be positioned on the table and secured with brackets and/or clamps. The table slides across a stainless steel axis and at the backend lies on an aluminum bar. This was done to ensure a statically determined construction. To make sure that the table does not move during an insertion a locking mechanism was created. Locking of the sliding motion can be done with a pin-hole connection at the back end of the table. The table with attached brackets ensures that the phantom does not move during insertion and after an experiment it can be easily unlocked and moved in increments of 10 mm and locked again. In case of a square block of gelatin this means that multiple insertions can be done in a reasonable amount of time without having to reposition the phantom itself on the table, ensuring that the boundary conditions have not changed.

One drawback of this design is that the needle will have an absolute position above the breadboard table of 20 mm which cannot be changed. Implementing the possibility of repositioning the phantom in height was considered but would make the design too complicated with respect to the added value of this feature. Further, the thickness of the phantom is, according to the requirements, 40 mm which would mean that the needle is inserted at the exact middle of the phantom.

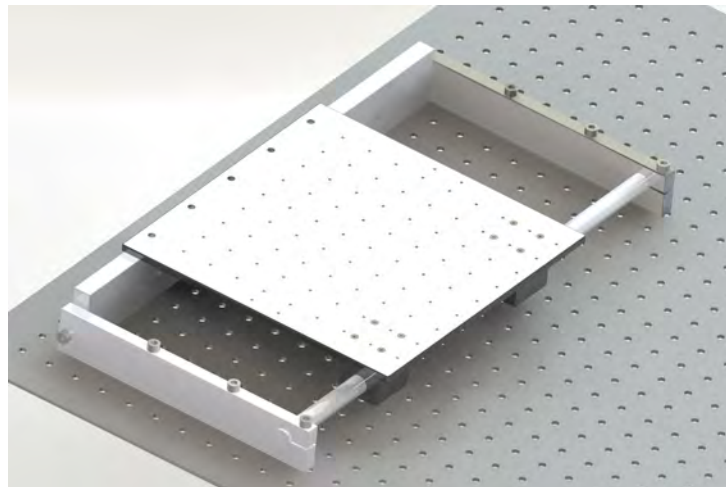


Figure 2.4: Manual slide table

2.5 Construction of the NID

After the design was finished the parts were ordered and construction of the needle insertion device could begin. In Figure 2.1 the final result can be seen. In this section it is explained how the NID is actuated and controlled. Further, a proof of principle is given which indicates that the device is working according to the specifications and requirements.

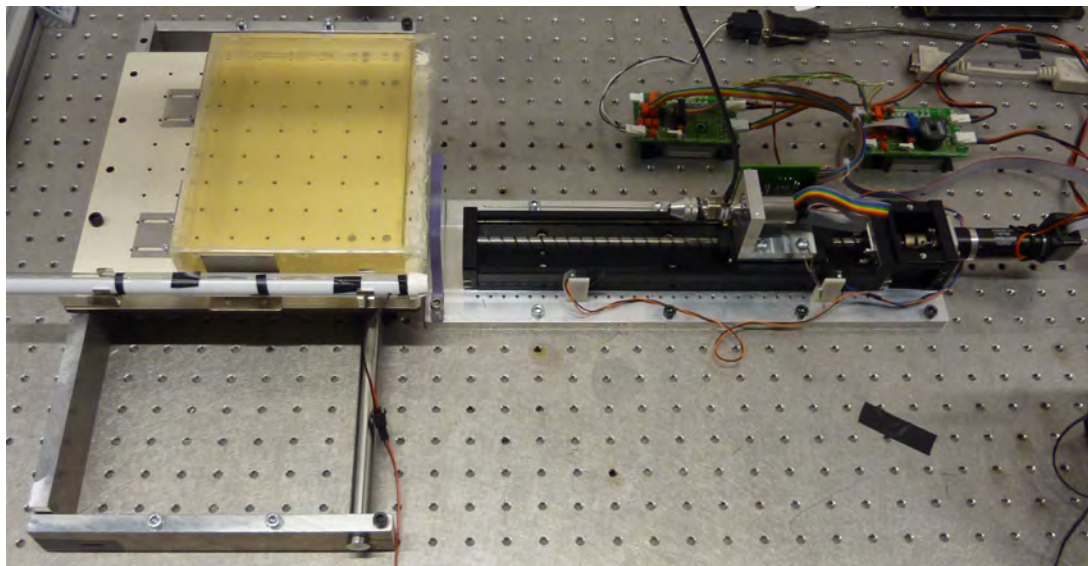


Figure 2.5: The needle insertion device as it has been constructed in the lab. The Elmo controllers are clearly visible as well as the linear stage and the manual sliding table with a block of gel mounted on it. The CCD cameras are not shown.

2.5.1 Control and actuation of the NID

After the construction a great amount of time was spent in writing the necessary software to control and actuate the NID. The following section describes the software and hardware structure which actuates and controls the two motors and receives data from the camera or ultrasound device and force/torque sensor as shown in Figure 2.6. The main environment in controlling the motion of the needle and receiving data from the sensor and camera is Matlab (v7.11, Mathworks Inc. Natick, USA) which is installed on a PC. Via the Matlab Data Acquisition Toolbox and a DAQ card a connection is made with the nano17 F/T sensor. Via the Matlab Image Acquisition Toolbox another connection is made with the CCD cameras, or an UltraSound device. Data from both the camera/US device and nano17 F/T sensor is stored in separate files in the Matlab environment available for post-processing. Actuation and control of the motors is done via the two Elmo controllers which are connected to Matlab via two USB-to-RS232 cables. The user inputs which type of motion must be performed and defines the necessary parameters. These parameters are the type of motion, which can be any combination of a continuous or tapping insertion with or without rotation, the insertion velocity and endposition of the translation, the number of tapping steps if tapping is applicable and the frequency and angular displacement of the rotation. Rotation is in this case a sinusoidal motion with a frequency and angular displacement. Full rotation is not possible due to the cable of the nano17 F/T sensor which would wind up around the needle.

This information is then send to the controllers and the nano17 F/T sensor and camera are turned on. To ensure that the motions start at the same time, a connection between the digital inputs and outputs of the controllers is made. Inside the controller software a synchronization point is made where one controller waits for a signal from the other and when it is ready they start at the same time with their respective programmed motions. Inside the controllers a recorder is implemented that records the position and velocity of the two motions. After a motion has ended the controllers send the position and velocity

data back to Matlab in a hexadecimal IEEE 32bit floating point format. A function was written that transforms the hexadecimal format to decimal numbers which are then stored in a separate file on the PC.

So to conclude, after one experiment the following data is available for post-processing

- A video recording of the insertion either with a CCD camera or ultrasound device.
- Force and torque data from the nano17 F/T sensor.
- Position and velocity data of the two degrees of freedom.

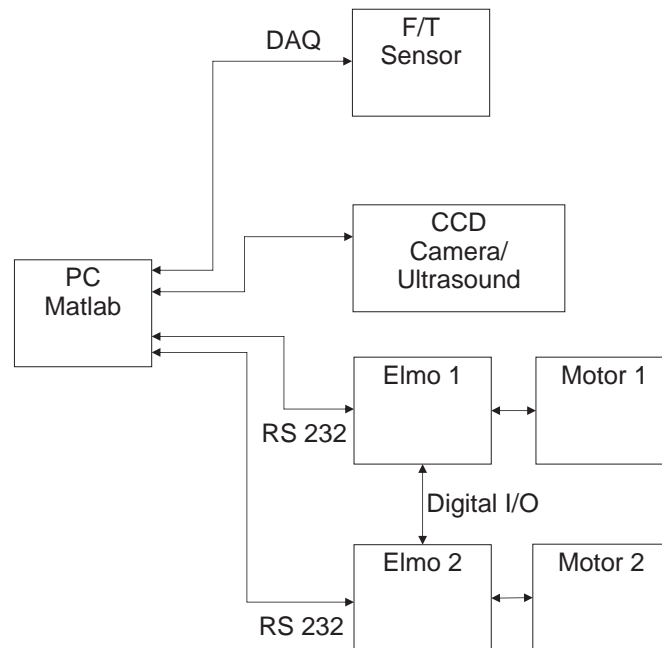


Figure 2.6: Control Structure NID

2.5.2 Sinusoidal motion generation

The rotation motion consists of a sinusoidal position profile with a frequency and angular displacement. Full rotation is not possible due to cable wind up of the nano17 F/T sensor. An abnormality was found which results in the rotation not performing according to the desired frequency. As a result the motion is rotating on a different frequency and is not smooth whenever more than one full period is performed. This problem and the implemented solution is mentioned here.

To accurately perform a sinusoidal position profile a number of setpoints have to be sent from the PC to the controllers. Sending every setpoint to the controllers during the motion results in inaccurate position profiles due to the non-realtime nature of RS232 communication in combination with the Windows operating system. This results in setpoints being sent too late to the controller which makes it impossible to have a smooth motion. Therefore it was decided to use a Position-Time(PT) array feature on the controller. This feature makes it possible to send an array of setpoints prior to the beginning of a motion. During the motion the controller interpolates a third degree order between all the setpoints and performs a smooth motion. However this created another problem being that the desired frequency of the sinusoidal motion could not be matched exactly with the controller sampling time. This will be explained with an example. The controller sampling time equals 360 microseconds, this means that

every 360 microseconds the controller takes a setpoint from the PT array, interpolates with the previous samplepoint and performs the motion. For a 1 Hz sinus profile this means that for one period the controller should fit $1/3.6e^{-4}=2777.8$ samples in the PT array. This is impossible and results in either 2778 points being stored in the array which means it has a small added length, or it stores 2777 points in the array in which case it is missing a certain part of the motion. The difference is quite small but whenever more than one period of a sinusoidal motion is performed the end of the first period and the beginning of the second period don't match correctly which results in an irregular motion. Also the performed frequency is slightly different than the desired frequency. To solve this problem an optimization algorithm was written which would take the desired frequency and search for the frequency which is closest to it, but fits with an integer number of samplepoints in the PT array. It does this while maintaining at least 110 points in the PT array to ensure a smooth motion. This number was obtained by trial and error and found to be adequate. For the example mentioned above this means a frequency of 1 Hz becomes a frequency of 1.00064 Hz.

This method ensures that when multiple periods of a rotation are performed sequentially, the beginning and end of the PT array match correctly resulting in a smoother motion. Another option would have been to change the number of stored periods in the PT array but due to limitations in memory of the controller no more than 1024 samplepoints can be stored inside the PT array. In some combinations of rotation frequency and number of sequential periods this limit is reached. For example, to perform a 1 Hz motion smoothly, one period needs at least 110 samplepoints in the PT array. If the insertion time equals 10 seconds this means that 10 rotations are performed. Thus 1100 samplepoints are needed in the PT array which is not possible.

Also changing the controller sampling time to a more logical number than 360 microseconds was considered, however this still introduced the same problem with certain other frequencies between 0.1 and 5 Hz. It is concluded that the difference in desired and actual frequency is small (maximum $\sim 0.1\%$) and that it will not be a great influence on the intended motion but this solution does result in a smooth motion with frequencies between 0.1 and 5 Hz.

2.5.3 Proof of principle

A number of experiments were performed to validate the constructed device with the specifications and requirements which were mentioned in Section 2.3. The parameters for the experiments are shown in Table. 2.1. The maximum rotation frequency that was chosen equals 5 Hz. For this frequency the maximum velocity equals 300 rpm which is the specified maximum rotational velocity as mentioned in Section. 2.3.

Experiment #	Insertion		Rotation (sinusoidal)	
	Insertion velocity (mm/s)	Insertion depth (mm)	Angular displacement (deg)	Frequency (Hz)
1	300	100	not applicable	not applicable
2	not applicable	not applicable	$\pm 90^\circ$	1
3	not applicable	not applicable	$\pm 90^\circ$	5
4	300	100	$\pm 90^\circ$	5

Table 2.1: Motion profiles for Proof-of-Principle

experiment #1

The first experiment is performed to check whether the device can insert a needle at the maximum insertion velocity of 300 mm/s with an acceleration of 10 m/s². In Figure 2.7 the result of this experiment is shown. It is concluded that the device follows the desired motion profile correctly. The needle accelerates with the required 10 m/s². The overshoot of the velocity profile equals 16.8 mm/s (= 5.6%) and is considered to be acceptable.

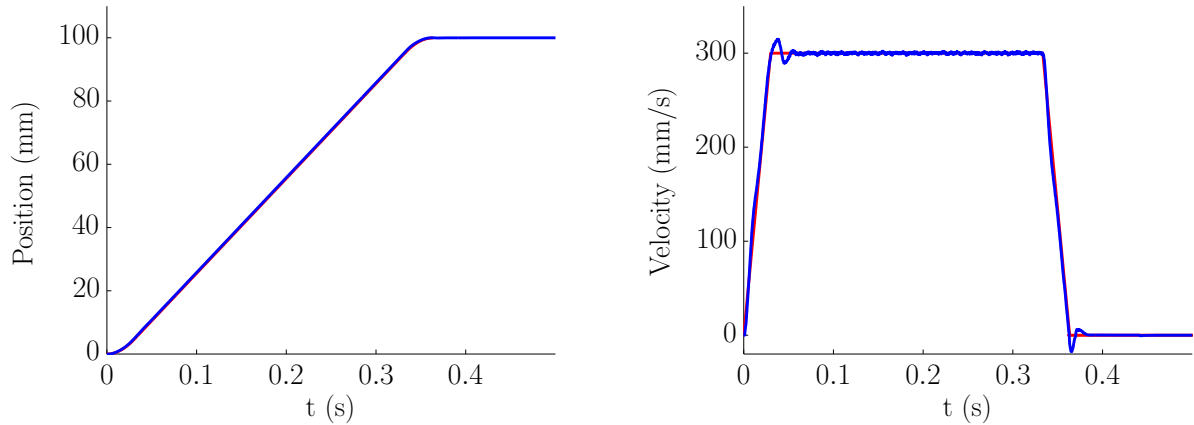


Figure 2.7: Position and velocity profile of translation with a velocity of 300 mm/s. The desired motion profile (red) vs. actual motion profile (blue). The maximum velocity error equals 16.8 mm/s at the overshoot peak.

experiment #2

The second experiment was performed to see whether the device can rotate a needle at 1 Hz with an angular displacement of $\pm 90^\circ$ degrees. In Figure 2.8 the result of this experiment is shown. The maximum position overshoot equals 0.18° (= 0.2%). The velocity profile is showing a noisy signal but this is due to the differentiation of the discrete position signal. It is concluded that the device is able to perform the desired motion profile correctly.

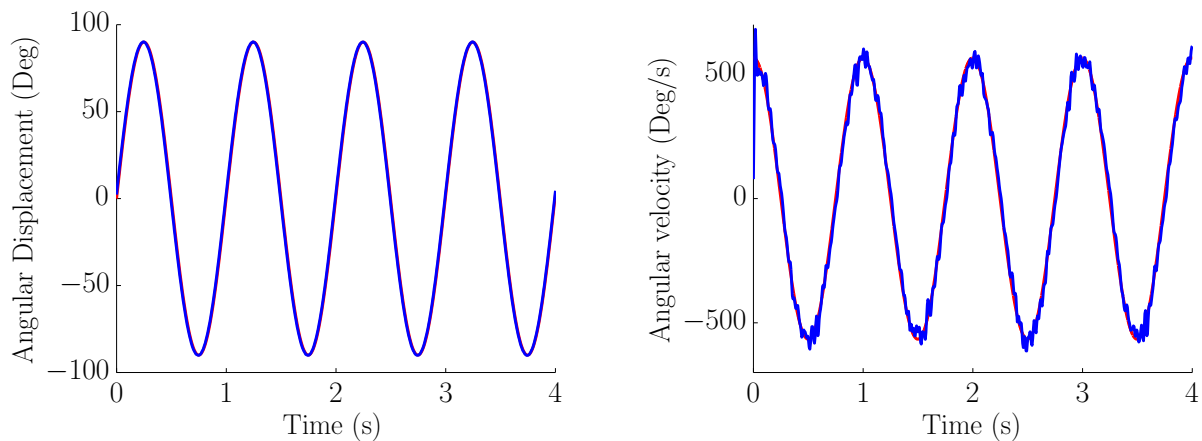


Figure 2.8: Sinusoidal position profile with a frequency of 1 Hz and an angular displacement of $\pm 90^\circ$ (left) with resulting velocity profile (right). Desired motion profile (red) vs. actual motion profile (blue). The maximum position overshoot equals 0.18° .

experiment #3

The third experiment was performed to see whether the device can rotate a needle at 5 Hz with an angular displacement of $\pm 90^\circ$ degrees during an insertion. In Figure 2.9 the result of this experiment is shown. The maximum position overshoot equals 1° ($\sim 1\%$) which is acceptable. It is concluded that the device can perform a 5 Hz rotation with an angular displacement of $\pm 90^\circ$ correctly.

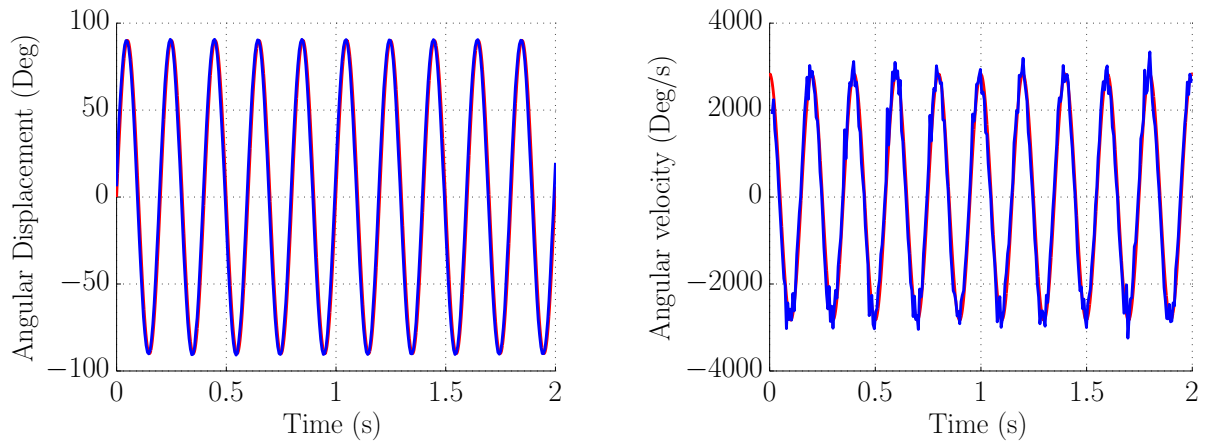


Figure 2.9: Sinusoidal position profile with a frequency of 5 Hz and an angular displacement of $\pm 90^\circ$ (left) with resulting velocity profile (right). Desired motion profile (red) vs. actual motion profile (blue). The maximum position overshoot equals 1° .

experiment #4

The fourth experiment was performed to see whether the device can combine the two motions of a translation of 300 mm/s and a rotation of 5 Hz with an angular displacement of $\pm 90^\circ$. In Fig. 2.7 the translation phase can be seen and in Fig. 2.10 the rotation phase can be seen. The maximum position overshoot is 1° as in experiment #3 and it is concluded that the device is capable of performing the desired motion profile.

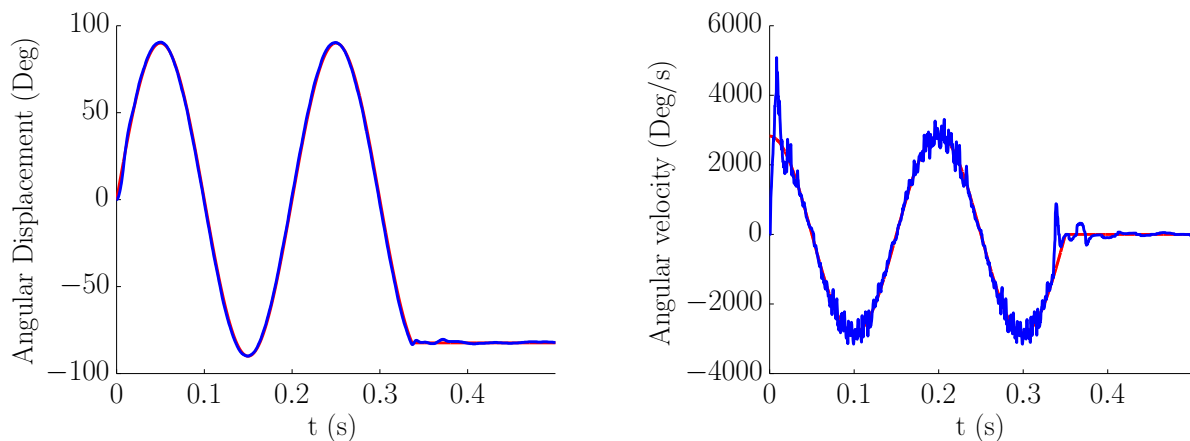


Figure 2.10: Sinusoidal position profile with a frequency of 5 Hz and an angular displacement of $\pm 90^\circ$ (left) with resulting velocity profile (right). Desired motion profile (red) vs. actual motion profile (blue). The maximum position overshoot equals 1° .

2.5.4 Conclusion

From the experiments it is concluded that the device works according to the specifications and requirements with regard to the desired velocities for translation and rotation. The device as built also complies with the other requirements and wishes and thus it can be used for experimentation.

Chapter 3

Macroscopic Observations of Needle-Tissue Insertions

A part of the assignment consisted of performing experiments with the goal of making macroscopic observations on the needle-tissue interaction. The goal of the experiments was to detect the influence of certain parameters on the deflection of a needle during an insertion. The parameters in question were the insertion velocity, the needle diameter, the bevel angle, needle tip shape, gel elasticity and motion profile. The results of these experiments were combined with a microscopic study which looked at microscopic effects happening at the tip of a needle during insertion. All results were written in the form of a journal paper which will be send to the *Medical Engineering and Physics* journal. For the purpose of this thesis it must be pointed out that the author of this thesis was responsible for, and performed all the macroscopic experiments. Further, a leading role was taken in writing this paper. The paper is shown in the following pages.

Macroscopic and Microscopic Observations of Needle Insertions in Soft Tissue

Youri van Veen, Alex Jahya*, Sarthak Misra
MIRA - Institute of Biomedical Technology and Technical Medicine
University of Twente, The Netherlands.
* email: A.Jahya@utwente.nl

3.1 Abstract

During a needle insertion into soft tissue, interaction occurs between the needle and the tissue. When a thin needle with a bevel tip is used, the needle will bend during insertion due to an asymmetric distribution of forces at the needle tip. In this study macroscopic and microscopic observations are made on the interaction between needle and tissue. Several parameters were subject to research to detect their influence on the interaction between needle and tissue. These parameters include, insertion velocity, needle diameter, needle bevel angle, gel elasticity, needle tip shape and type of motion profile during insertion. Results show that increasing the insertion velocity results in a higher insertion force and lower amount of needle deflection. Increasing the needle diameter results in less needle deflection and higher insertion force due to a higher second moment of inertia. Varying the needle's bevel angle between 8° and 82° reveals a nonlinear trend with regard to insertion force and needle deflection. This is due to a synergy between compression and cutting actions which are observed on a microscopic level at the needle tip. Increasing the gel elasticity results in more needle deflection and higher insertion force. Needle tip shape results show that a bevel tip results in the highest amount of needle deflection but that insertion force is equal for the tested tip shapes. Different motion profiles were performed and results show that adding a 1 Hz rotation to an insertion decreases the amount of needle deflection. Increasing the angular velocity from 1 Hz to 5 Hz decreases the amount of insertion force while the amount of needle deflection remains the same. A tapping motion was performed but yielded no significant decrease in needle deflection and a slight increase in insertion force.

3.2 Introduction

Percutaneous needle insertion is one of the most common minimally invasive medical procedures that is performed for local drug delivery, brachytherapy and biopsy. Accurate needle placement in these procedures is of importance, mainly because biopsy of an unintended tissue region can result in misdiagnosis, or in case of brachytherapy, malignant tissue is not destroyed. Inaccuracy of needle placement can be caused by several factors such as tissue inhomogeneity, tissue anisotropy, anatomical obstructions during needle insertion, and physiological processes like fluid flow and respiration. Such targeting error can be reduced by using a robot to insert and steer a needle towards a target. Several groups have investigated the use of robotic needle insertion devices ([2, 3, 8, 9, 10, 11, 15, 22, 35]). In order to control and accurately steer a needle towards a target, knowledge is required about the forces that act on the needle and how these influence the deflection of the needle.

The research that is performed by the previously mentioned groups, are observations of parameters that influence the needle-tissue interaction. These parameters include, among others, insertion velocity, needle diameter, bevel angle, tip shape, gel elasticity and motion profile. Observations are made on the macroscopic effects during needle insertion like needle deflection, target deformation or the forces acting on the entire needle. For instance Lagerburg et al. [15] investigated a tapping insertion method to minimize motion of the prostate. Their results show that with a high velocity tapping insertion, the mean prostate motion can be diminished from 5.9 mm to 0.9 mm. However they did not look at deflection of the needle during an insertion. Abolhassani et al [1] studied different insertion methods of a bevel tip needle to diminish needle deflection and found that rotation decreases the amount of needle deflection. Podder

et al. [28] studied different insertion and angular velocities and what their effects were on measured forces on the base of the needle and the target deformation. They used a diamond tip shaped needle and did not investigate the amount of needle deflection. For the earlier mentioned purpose of navigating a needle through a soft tissue, it has been found by Okamura et al [23] that a bevel tip shape results in the highest amount of deflection and thus would be suitable for steering.

This study has the goal to see how different parameters have an effect on needle deflection. This information can be used in models on the needle-tissue interaction or for projects in which the needle is navigated around objects. Macroscopic experiments are performed which look at the entire needle during insertion. However it is also important to look at microscopic effects of the needle-tissue interaction. Misra et al. [22] observed the tip of a needle during an insertion using a confocal microscope to study the rupturing processes of a needle tip cutting through a soft tissue.

In this study a set of microscopic experiments is performed to see how the previously mentioned parameters have an effect on the rupture processes acting at the needle tip. The paper is organized as follows: Section 3.3 describes the used experimental setups and experiments that were performed. In Section 3.4 experimental results are given. Finally Section 3.5 provides conclusions and directions for future work.

3.3 Experimental Setup

In the following sections the experimental setups for the macroscopic and microscopic experiments are shown and described. Further, the experiments that are performed are described.

3.3.1 Macroscopic Study

Experimental Setup

A two degrees-of-freedom (DOF) needle insertion device (shown in Fig. 3.1) is designed for the macroscopic experiments. It allows translation along and rotation about the needle's longitudinal axis. The device consists of a Misumi translation (type LX3010) stage (MISUMI Group Inc. Tokyo, Japan) actuated with a Maxon Motor (type RE25, with GP26B gearhead, transmission ratio 4.4:1), and a needle rotational setup using a Maxon Motor (type ECTMax22)(Maxon Motor, Sachseln, Switzerland). Both motors and thus the motion are controlled using the position controller on two Elmo Whistle 2.5/60 controllers (Elmo Motion Control Ltd, Petach-Tikva, Israel). Measurement of forces acting on the needle during insertion is done with a six-axis nano17 force/torque sensor (ATI Industrial Automation, Apex, USA) located at the base of the needle. Moreover, needle insertion is recorded at 30 fps via a Sony XCD-SX90 charge-coupled device (CCD) FireWire camera (Sony Corporation, Tokyo, Japan) mounted at a height of 450 mm from the top surface of the gel. Matlab (v7.11, Mathworks Inc., Natick, USA) was used to interface the camera, the nano17 sensor and the Elmo controllers. The device is capable of reaching accelerations of 10 m/s² and can insert a needle with a maximum velocity of 300 mm/s. The maximum angular velocity is 300 rpm. A tracking algorithm based on the work of Xiao et al. [36] is applied to the recorded movies to extract the amount of needle deflection.

Experiment Plan

The parameters that are investigated include insertion velocity, bevel angle, needle diameter, gel elasticity, motion profile and needle tip shape. The different experimental parameters are shown in Table 3.1. All needle insertions are performed on a phantom made from gelatin with varying mixtures gelatin-to-water. The mixtures used are a 8%, 14.9% and 20% masspercentage gelatin-to-water mixture. Gel blocks were made and left in the refrigerator for 16 hours after which they were taken out and left for 4 hours to warm up to room temperature. Needles were made from stainless steel wire. A disc polisher was used to create different needle tips. Tip shapes were viewed under a microscope and the tip angle was found to be accurate within 2° of the intended angle.

The measurements include insertion force data measured at the base of the needle and the amount of needle tip deflection.

Experiment #1 is a study on insertion velocity. The insertion velocity is varied between $v = 5$ mm/s to 300 mm/s. Experiment #2 is a study on the effect of different needle diameters which were chosen to be $\phi = 1$ mm, $\phi = 1.6$ mm and $\phi = 2$ mm. These diameters correspond with actual biopsy needles used in prostate biopsy or breast biopsy. Experiment #3 is a study on a number of different bevel angles between $\beta = 8^\circ$ and 82° . Experiment #4 is a study on gel elasticity. Three different gelatin elasticities (Table. 3.2) were used of which the elasticity was determined by performing a uniaxial compression test using the Anton Paar Physica MCR501 (Anton Paar GmbH, Graz, Austria). The three values represent elasticity values of prostate tissue found in the human body [14]. Experiment #5 is a study on different needle tip shapes and their effects on insertion force and needle deflection. The used tip shapes can be seen in Fig. 3.2 and are a diamond tip, a franseen tip, a conical tip and a bevel tip shape. Experiment #6 is a study on different motion profiles. The profiles used are a continuous insertion without rotation and with rotation. Rotation is a sinusoidal motion with a frequency between 1 and 5 Hz and an angular displacement of 180° . Full rotation was not possible due to wind-up of the nano17 sensor wire. A high velocity tapping motion is also performed in which the needle is inserted in steps of 20 mm with a velocity of 250 mm/s and 300 mm/s.

3.3.2 Microscopic Study

Microscopic observations of needle-tissue interactions at the needle tip is done using a single DOF planar insertion device and a Zeiss Laser Scanning Confocal Microscope (LSCM) 510 microscope (Fig. 3.3). Needle tip and the gelatin phantom are visualized with differential interference contrast (DIC), epifluorescence using 488 nm line of argon laser, and 10x objective lens. DIC imaging enhances the contrast of the rupture, while epifluorescent imaging augments the visibility of air bubble presence. To facilitate epifluorescent imaging, the gelatin is doped with fluorescein isothiocyanate (FITC).

The needle (inset of Fig. 3.3) is mounted on a 6-DOF force/torque sensor (ATI nano17) with force and torque resolution of 12.5 mN and 0.0625 Nmm, respectively. Solid needles of diameter 1 mm and 1.6 mm and of bevel angle 30° , 60° and 75° are used in the experiment. Two stoppers are used to prevent movement of the gelatin; hence, the recorded forces and torques solely result from needle-gelatin interactions. Force and torque data are sampled at 2000 Hz using National Instrument's LabViewTM data acquisition software. It is then averaged to reduce sampling noise. In this experiment, the needle is inserted at two velocities, $v = 0.5$ mm/s and 1 mm/s. Moreover, fracture or crack are imaged in 2 and 3-dimensions (2D and 3D) with a resolution of 512 x 512 pixels.

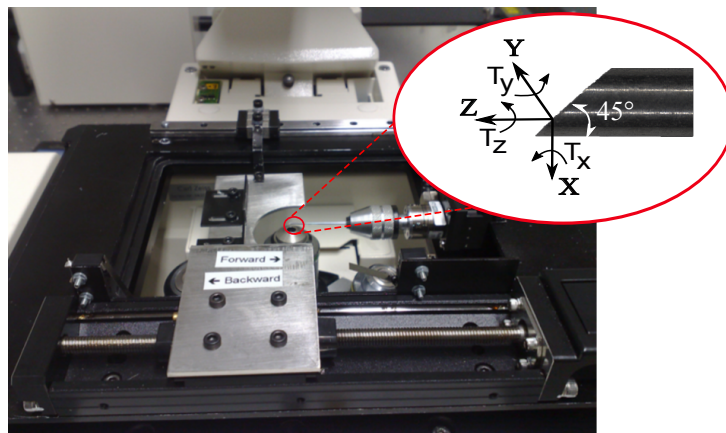


Figure 3.3: Experiment setup for observing microscopic needle-gel interaction under laser scanning confocal microscope (Inset shows the needle tip with $\beta = 45^\circ$).

3.4 Observations and Results

In this section the observations and results of the performed experiments are described. First the macroscopic experiments are mentioned followed by the microscopic results. Each combination of parameters, as shown in Table 3.1, results in an insertion which is performed three times. The average of the three samples is shown in the different plots. The measurements contain insertion force data obtained from the ATI nano17 sensor and needle tip deflection data obtained from processed camera images.

3.4.1 Macroscopic Observations of Needle-Tissue Interactions

Experiment #1 The effect of different insertion velocities is investigated in experiment #1(Fig. 3.4). The maximum insertion force ($|F_{z,max}|$) increases by 226% with the insertion velocity increasing from $v = 5$ mm/s to 300 mm/s, while the maximum needle tip deflection ($|\delta_{max}|$) decreases by 10% for the same increase in insertion velocity. $|F_{z,max}|$ and $|\delta_{max}|$ asymptotically approached 6 N and 7.8 mm with increasing insertion velocity, respectively.

Experiment #2 The effect of varying needle diameter is investigated in experiment #2(Fig. 3.5). Increasing the diameter of the needle from $\phi = 1$ mm to $\phi = 2$ mm results in an increase of 126%, 120% and 98% of $|F_{z,max}|$ for insertion in gelatin with elasticity E_1 , E_2 and E_3 , respectively. For the same increase in needle diameter $|\delta_{max}|$ decreases by 50%, 31% and 52% for E_1 , E_2 and E_3 , respectively. The decrease of $|\delta_{max}|$ is due to a higher second moment of inertia of the needle which represents the resistance to bending. The second moment of inertia of the needle increases with a factor of ϕ^4 (3.1).

$$I_{needle} = \frac{\pi\phi^4}{64} \quad (3.1)$$

Experiment #3 In experiment #3 the effects of varying the bevel angle is investigated(Fig. 3.7). A nonlinear trend is found for both $|F_{z,max}|$ and $|\delta_{max}|$. From $\beta = 8^\circ$ to 30° , $|\delta_{max}|$ increases by 104% and then drops 32% for $\beta = 65^\circ$. From $\beta = 65^\circ$ up to 82° the needle deflection increases by 34%. From $\beta = 8^\circ$ to 82° , $|F_{z,max}|$ increases 59%. The nonlinear trend is explained by observations on the rupture effects at the needle tip which are mentioned in subsection 3.4.2.

Experiment #4 In experiment #4 varying the gel elasticity is investigated(Fig. 3.5). Increasing the gel elasticity from E_1 to E_3 results in an increase of $|F_{z,max}|$ of 502%, 420% and 427% for the cases of $\phi = 1$ mm, $\phi = 1.6$ mm, and $\phi = 2$ mm, respectively. For the same increase in gel elasticity, $|\delta_{max}|$ increases by 40% and 49% for $\phi = 1$ mm and $\phi = 1.6$ mm, respectively. For the case of $\phi = 2$ mm it is shown that $|\delta_{max}|$ increases by 34% from E_1 to E_3 but $|\delta_{max}|$ is larger for E_2 than for E_3 . This is due to a gel rupture effect which is not observed with gel elasticities below E_3 . With the stiffest gel(E_3) and largest diameter(2 mm) it is observed that there are sudden drops in insertion force corresponding with an axial crack occurring from the insertion point along the needle shaft. This crack decreases the contact area of the gelatin and needle and therefore the friction force decreases which results in a relaxation phase which in return results in less deflection of the needle. In Fig. 3.6 two needle diameters of $\phi = 1$ mm and $\phi = 2$ mm were inserted into a gelatin phantom. After 10 seconds the motion is stopped and a relaxation phase is seen. The decreased insertion force which occurs due to a crack is clearly seen with $\phi = 2$ mm by two sudden drops in insertion force (F_z).

Experiment #5 The effects of different tip shapes is investigated in experiment #5(Fig. 3.8). Results show that $|F_{z,max}|$ is relatively equal(~ 2.8 N) for all tip shapes. This is because the insertion force is mostly dependent on the friction along the shaft which is the equal for all needle tip shapes. The bevel tip shape results in the highest amount of $|\delta_{max}|$ of 8.8 mm which is due to the asymmetric force distribution on the tip. The needle tip deflection of the symmetric shapes of the conical,fransen and diamond tip are due to small inaccuracies in straightness of the needle or a slight deviation from a straight insertion into the gel.

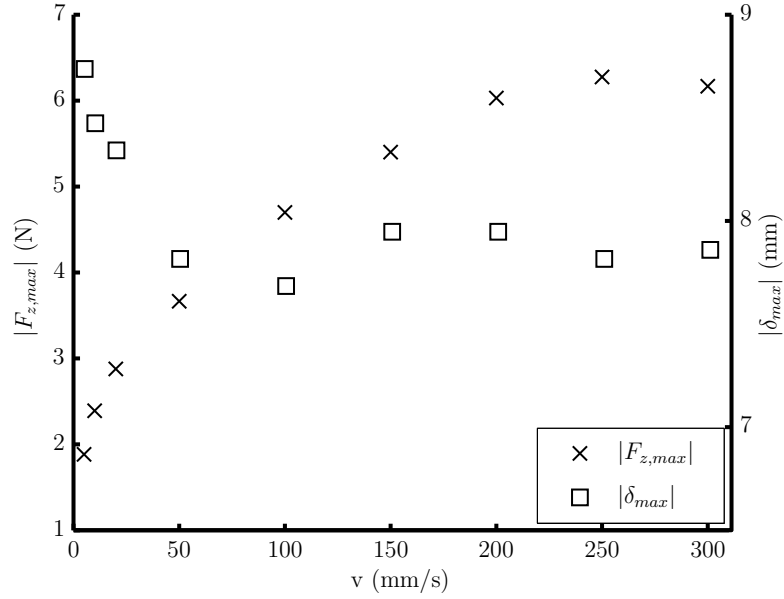


Figure 3.4: Maximum insertion force ($|F_{z,max}|$) and maximum needle tip deflection ($|\delta_{max}|$) for different insertion velocities (v). The insertion distance is 100 mm, the gel elasticity is $E_2 = 35.5$ kPa and needle diameter and bevel angle are 1 mm and 30° , respectively. The average standard deviations are 0.08 N and 0.18 mm for $|F_{z,max}|$ and $|\delta_{max}|$, respectively.

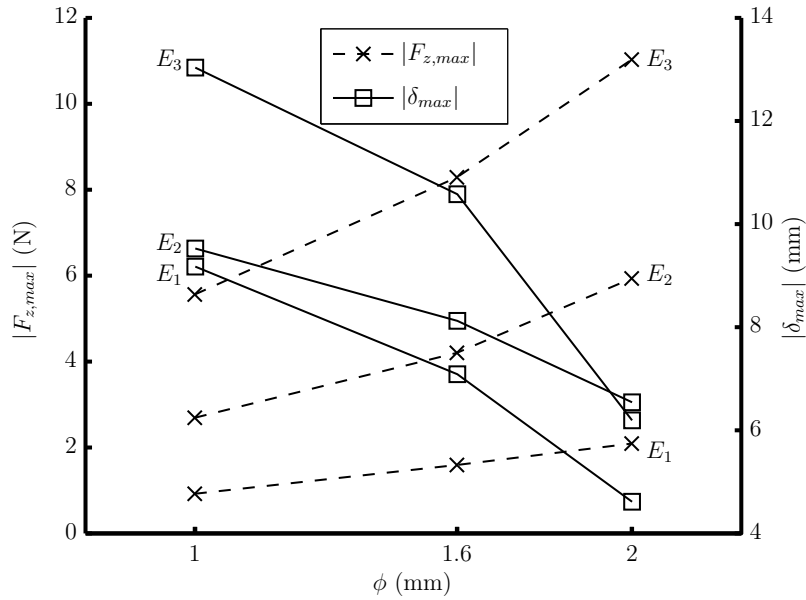


Figure 3.5: Maximum insertion force ($|F_{z,max}|$) and maximum needle tip deflection ($|\delta_{max}|$) results with varying needle diameter and gel elasticity. The different gel elasticities are $E_1 = 8.7$ kPa (softest), $E_2 = 35.5$ kPa and $E_3 = 58.1$ kPa (stiffest) and the needle diameter is $\phi = 1$ mm, $\phi = 1.6$ mm and $\phi = 2$ mm. The insertion distance is 100 mm, the insertion velocity is 10 mm/s, and bevel angle is 30° . The average standard deviations are 0.22 N and 0.39 mm $|F_{z,max}|$ and $|\delta_{max}|$, respectively. The data points are connected for clarity.

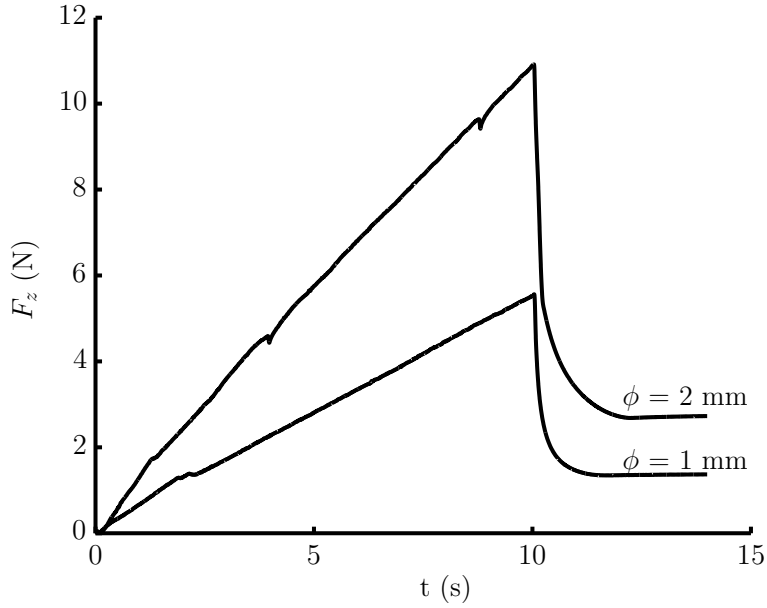


Figure 3.6: Insertion force (F_z) versus time (t) of a needle insertion into a gelatin phantom. Two needle diameters are shown being $\phi = 1$ mm and $\phi = 2$ mm. The insertion distance is 100 mm, the insertion velocity is 10 mm/s, the gel elasticity is $E_2 = 35.5$ kPa and bevel angle is 30° . The drops in force for $\phi = 2$ mm are due to formation of a crack perpendicular to the insertion direction. After 10 seconds the motion is stopped and a relaxation phase is clearly visible.

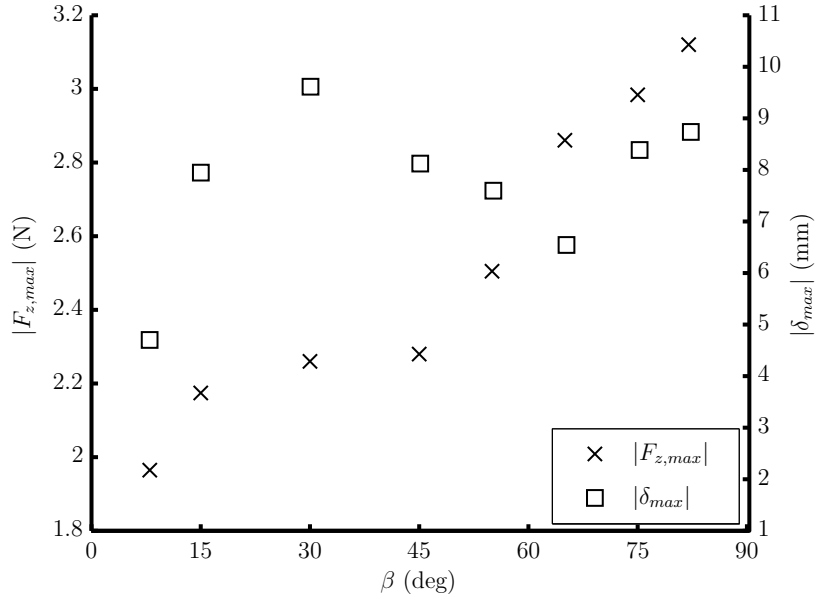


Figure 3.7: Maximum insertion force ($|F_{z,max}|$) and maximum needle tip deflection ($|\delta_{max}|$) results with different bevel angles. The insertion distance is 100 mm, the gel elasticity is $E_2 = 35.5$ kPa, the insertion velocity is 10 mm/s and needle diameter is 1 mm. The average standard deviations are 0.08 N and 0.15 mm for $|F_{z,max}|$ and $|\delta_{max}|$, respectively.

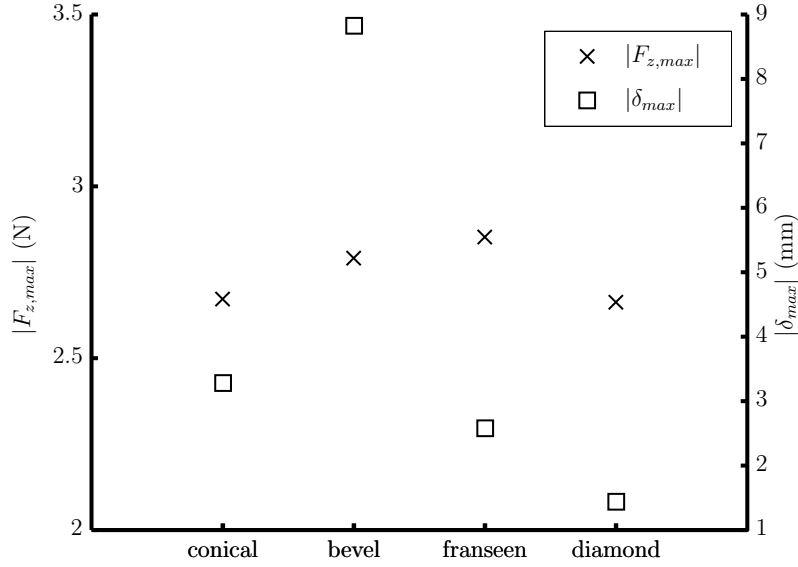


Figure 3.8: Maximum insertion force ($|F_{z,max}|$) and maximum needle tip deflection ($|\delta_{max}|$) results with different needle tip shapes. The insertion distance is 100 mm, gel elasticity is $E_2 = 35.5$ kPa, the insertion velocity is 10 mm/s and needle diameter is 1 mm. The average standard deviations are 0.14 N and 0.18 mm for $|F_{z,max}|$ and $|\delta_{max}|$, respectively.

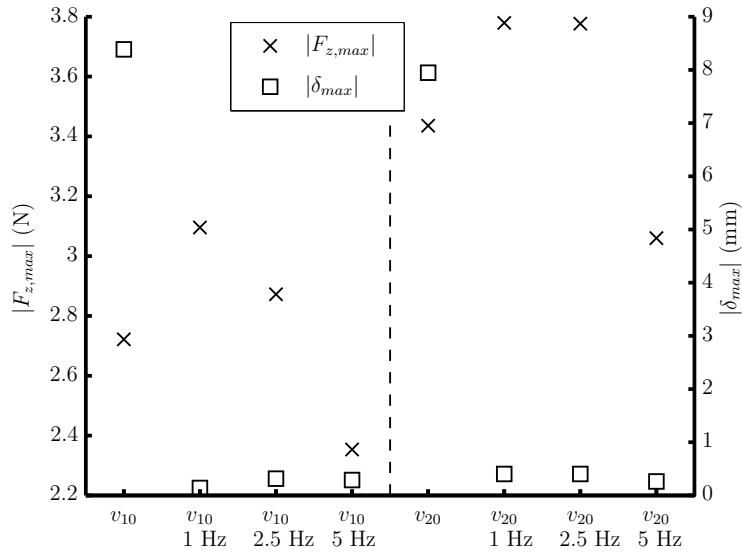


Figure 3.9: Maximum insertion force ($|F_{z,max}|$) and maximum needle tip deflection ($|\delta_{max}|$) results with different motion profiles. The profiles are v_{10} - continuous insertion ($v = 10$ mm/s) without rotation and $v_{10} + 1$ Hz, 2.5 Hz or 5 Hz - continuous insertion ($v = 10$ mm/s) with rotation with an angular velocity of 1 Hz, 2.5 Hz or 5 Hz. The same profiles are also performed where $v = 20$ mm/s ($v_{20} + 1$ Hz, 2.5 Hz or 5 Hz). The insertion distance is 100 mm, gel elasticity is $E_2 = 35.5$ kPa and needle diameter and bevel angle are 1 mm and 30° , respectively. The average standard deviations are 0.02 N and 0.18 mm for $|F_{z,max}|$ and $|\delta_{max}|$, respectively.

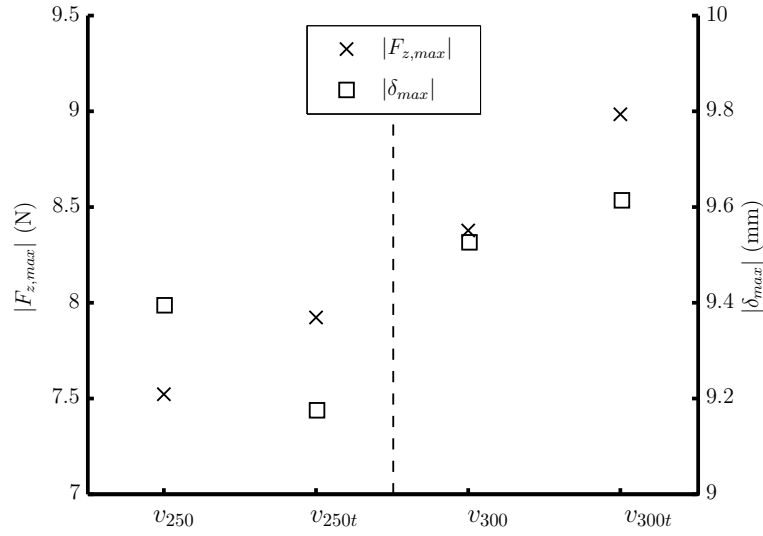


Figure 3.10: Maximum insertion force ($|F_{z,max}|$) and maximum needle tip deflection ($|\delta_{max}|$) results with different motion profiles. The profiles are v_{250} - continuous insertion ($v = 250$ mm/s), v_{250t} - tapping insertion ($v = 250$ mm/s), v_{300} - continuous insertion ($v = 300$ mm/s) and v_{300t} - tapping insertion ($v = 300$ mm/s). Tapping motion involves insertion in steps of 20 mm with a pause of 500 ms between each step. The total insertion distance is 100 mm. Gel elasticity is $E_2 = 35.5$ kPa and needle diameter and bevel angle are 1 mm and 30° , respectively. The average standard deviations are 0.25 N and 0.18 mm for $|F_{z,max}|$ and $|\delta_{max}|$, respectively.

Experiment #6 The effect of different motion profiles is investigated in experiment #6 (Fig. 3.9 and 3.10). As seen in Fig. 3.9, inclusion of a 1 Hz sinusoidal angular velocity to the insertion velocity $v = 10$ mm/s and 20 mm/s results in a 97% and 96% decrease in $|\delta_{max}|$, respectively. Adding a 1 Hz sinusoidal angular velocity results in an increase of 14% and 10% of $|F_{z,max}|$ for $v = 10$ mm/s and $v = 20$ mm/s, respectively. Increasing the angular velocity to 5 Hz decreases $|F_{z,max}|$ by 24% and 19% with respect to the 1 Hz case for $v = 10$ mm/s and $v = 20$ mm/s, respectively. $|\delta_{max}|$ does not change significantly with increasing angular velocities. The effect of tapping motion on needle deflection and insertion force is shown in Fig. 3.10. Results show that $|F_{z,max}|$ of the tapping motion increases by 5% and 7% for $v = 250$ mm/s and 300 mm/s, respectively. There is no discernible (~ 0.2 mm) change in $|\delta_{max}|$ for continuous versus tapping motion.

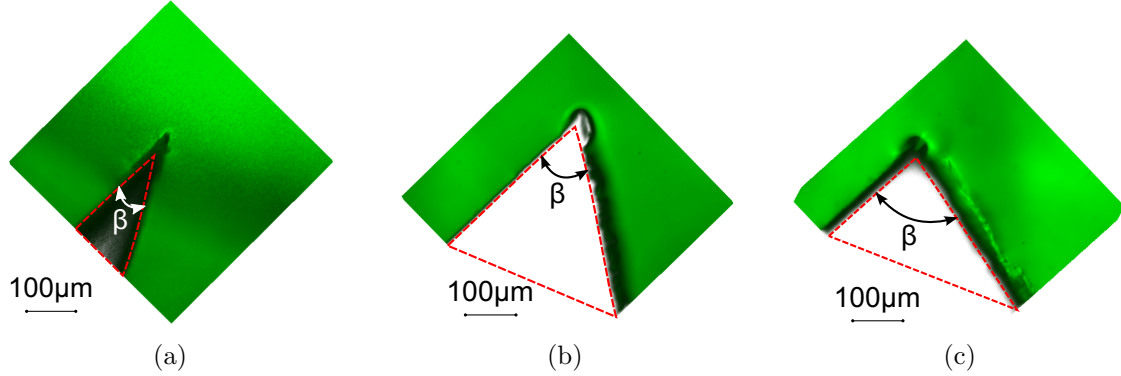


Figure 3.11: Tip crack for various bevel angles (β): (a) 30° , (b) 60° and (c) 75° . The dashed-line shows the needle's tip location. The tip crack is observed to be the longest and narrowest at $\beta = 30^\circ$ while it is the shortest and widest at $\beta = 75^\circ$.

3.4.2 Microscopic Observations of Needle-Gelatin Phantom Interactions

A microscopic study is performed to investigate the influence of gelatin rupture during needle insertion on the amount of needle bending. Two insertion velocities are chosen, $v = 0.5$ mm/s and $v = 1$ mm/s, these represent low and high insertion velocity, respectively. The insertion velocity can only be performed up to $v = 1$ mm/s due to hardware limitations.

It is noted that during needle insertion, mode-2 crack, or rupture occurs during needle insertion [22]. This occurrence of mode-2 rupture creates a tip rupture - a gap at the needle tip. Variation of the tip rupture with needle's bevel angle is shown in Fig. 3.11. Moreover, experimental result shows too that two actions occur during needle insertion. These actions are cutting and compression.

The tip rupture is noted to be narrow and long for a small bevel angle ($\beta = 30^\circ$), and becomes wider and shorter for a large bevel angle needle ($\beta = 75^\circ$). Further, it is noted that the increase in the needle's bevel angle results in a larger amount of compression (Fig. 3.12). This is due to the fact that a large bevel angle needle has a blunter tip, resulting in lesser cutting action during needle insertion.

The study between rupture images and force/torque data (Fig. 3.13) shows a relation between force/torque data to the occurrence of the tip rupture. The occurrence of a tip rupture is characterized by a sharp drop in the insertion force $|F_z|$ and deflecting torque along zy-plane $|T_x|$.

First, formation of the tip rupture (shown as slightly lighter-shade circular area at needle tip, Fig. 3.13 inset A) creates a space at the needle tip. This space allows $|F_z|$ acting at the needle bevel face to bend the needle further along the negative x-axis direction. This instance is indicated by the sharp increase of deflecting force and torque along zx-plane $|F_x|$ and $|T_y|$, respectively. Concurrently, this action reduces the contact between the tip and gel (resulting in the decrease of $|F_z|$), and allows the needle to deflect along the xy-plane back to its original shape/position (the decrease of $|T_x|$). Additional bending of the needle by $|F_z|$ creates a gap along the needle bevel face. This is shown in the lighter area around the needle's bevel face, Fig. 3.13 inset B. Moreover, the increase of the compression force in larger bevel angle needles result in the higher amount of $|F_z|$ (Fig. 3.14). At $\beta = 75^\circ$, coupling of high value of $|F_z|$ and large tip rupture gap translates to a large drop of $|F_z|$ and sharp increase of $|T_y|$. Further, the amount of increase of $|T_y|$ is noted to be higher than $\beta = 60^\circ$. Thus, the deflection noted at $\beta = 75^\circ$ is more than at $\beta = 60^\circ$.

Increase in the needle's diameter increases both surface area of the bevel face and the size of the tip rupture. This is shown by the higher amount of $|F_z|$ noted at $\phi = 1.6$ mm in comparison to a $\phi = 1$ mm needle for $\beta = 30^\circ$ (Fig. 3.15). In both cases, insertion velocity is at a constant value of $v = 0.5$ mm/s. Even though, higher amount of $|T_y|$ is noted for $\phi = 1.6$ mm, the needle deflection of a $\phi = 1.6$ mm needle is much less than a $\phi = 1$ mm needle. The increase in diameter results in more significant increase of needle's resistance to bending (second moment of inertia) in comparison to the increase in the amount of $|T_y|$ acting at the needle tip. In terms of variation of insertion velocity, insertion at $v = 1$ mm/s results in a lower amount of $|T_y|$. Thus, less deflection is noted at $v = 1$ mm/s than at $v = 0.5$ mm/s.

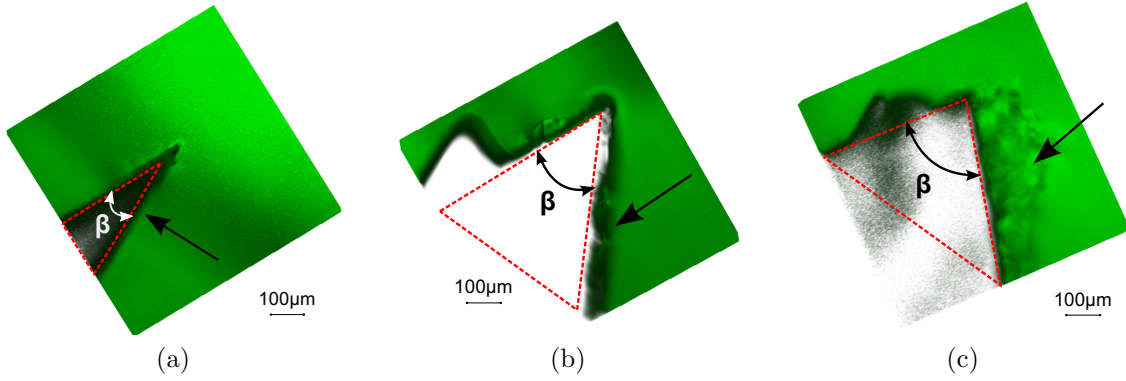


Figure 3.12: Compression of the gel (shown with an arrow) during needle insertion for various bevel angles (β): (a) 30° , (b) 60° and (c) 75° . The amount of compression is noted to be the most at $\beta = 75^\circ$.

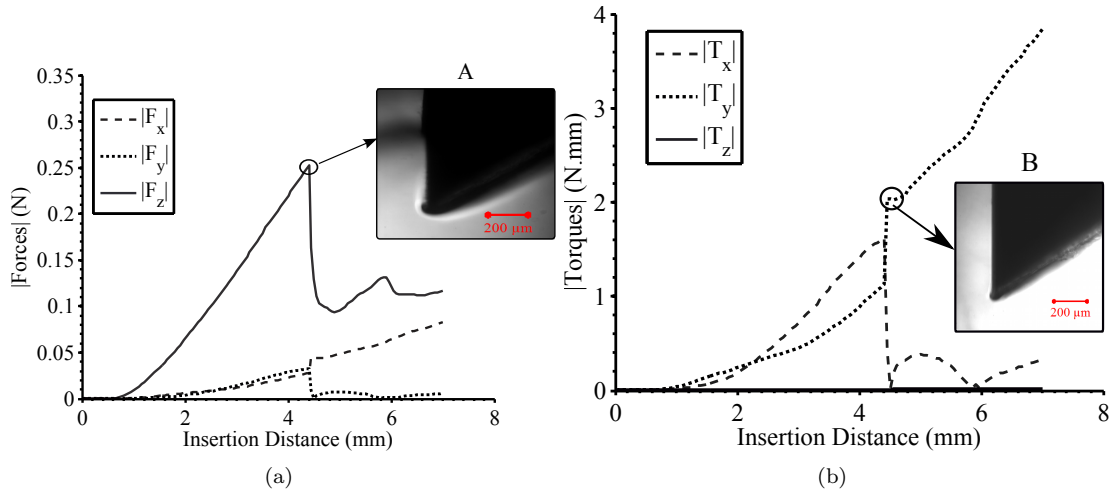


Figure 3.13: Forces and torques versus insertion distance for a needle insertion in a gelatin phantom. The insertion velocity is 0.5 mm/s , the needle's bevel angle is 60° and the gel elasticity and needle diameter are 35.5 kPa and 1 mm , respectively.

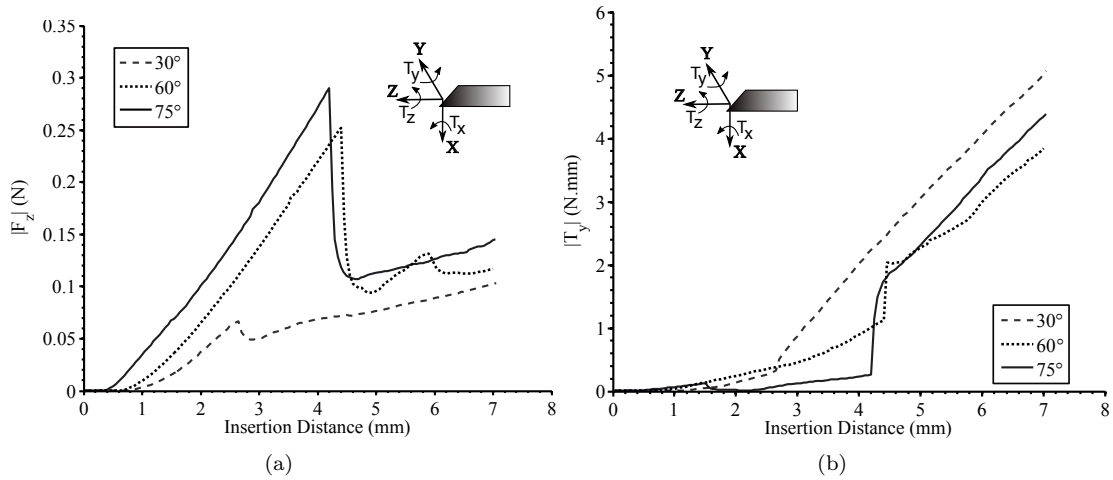


Figure 3.14: $|F_z|$ and $|T_y|$ versus insertion distance for needles with $\beta = 30^\circ$, $\beta = 60^\circ$ and $\beta = 75^\circ$. The insertion velocity is $v = 0.5 \text{ mm/s}$, gel elasticity and needle diameter are 35.5 kPa and 1 mm , respectively.

Moreover, since the effective stiffness of non-linear material increases with the rate of application of load, the increase in the insertion velocity results in the higher amount of $|F_z|$. Finally, experimental result of variations in gelatin elasticity is presented in Fig. 3.16. Lower ratio of gelatin powder to water results in the more elastic and softer gelatin; thus, smaller elastic modulus E . This translates to a lower amount of $|F_z|$ and $|T_y|$ acting at the needle tip for needle of $\beta = 30^\circ$ inserted at $v = 0.5$ mm/s

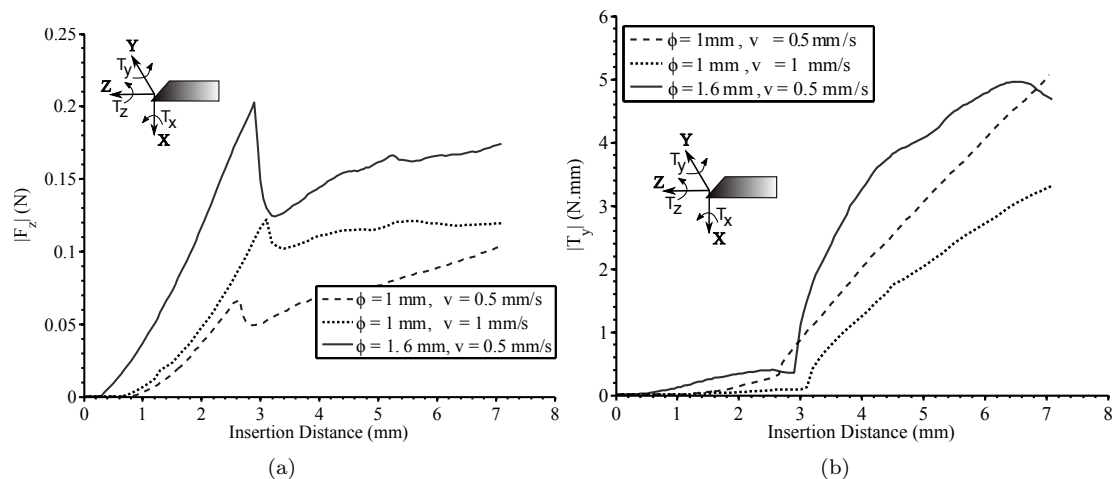


Figure 3.15: $|F_z|$ and $|T_y|$ versus insertion distance for $\phi = 1$ mm and $\phi = 1.6$ mm. $\phi = 1$ mm needle is inserted at $v = 0.5$ mm/s and $v = 1$ mm/s. Gel elasticity and bevel angle are 35.5 kPa and 30° , respectively.

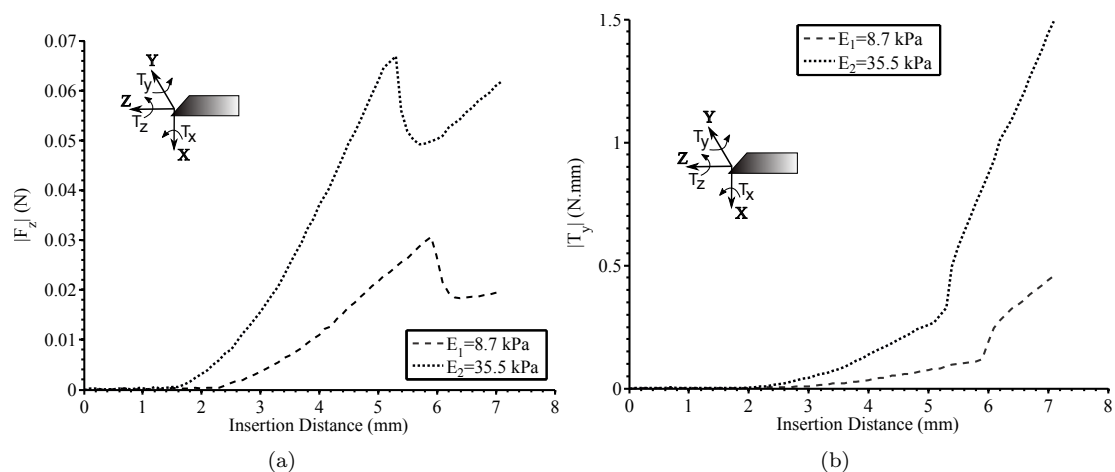


Figure 3.16: $|F_z|$ and $|T_y|$ versus insertion distance for different gel elasticities. Insertion velocity is 0.5 mm/s, gel elasticity is $E_1 = 8.7$ kPa and $E_2 = 35.5$ kPa, bevel angle and needle diameter are 30° and 1 mm, respectively.

3.5 Conclusion and Future Work

In this study, macroscopic and microscopic observations were done on needle insertions. Six parameters that have an influence on the needle tissue interaction were investigated. These parameters are insertion velocity, needle diameter, bevel angle, gel elasticity, needle tip shape and motion profile. It has been shown that increasing insertion velocity (from 5 mm/s to 300 mm/s) results in the insertion force asymptotically increasing from 1.9 N to 6 N. For the same increase in insertion velocity the maximum needle deflection asymptotically decreases from 8.7 mm to 7.8 mm. Increasing needle diameter (from 1 mm to 2 mm) results in less deflection but the insertion force increases. The second moment of inertia of the needle increases with larger diameter which means that the resistance to bending increases. This explains the diminished deflection of the needle.

Varying the bevel angle of the needles resulted in a nonlinear trend for insertion force and needle deflection which is explained by microscopic observations. It is observed that two actions, cutting and compression of the gelatin, happen during needle insertion. For small bevel angles ($\beta = 30^\circ$) it is shown that there is less compression of the gelatin compared to the large bevel angles ($\beta = 75^\circ$). More compression of the gel results in higher insertion force acting on the needle. It is also shown that for larger bevel angles ($\beta = 75^\circ$) the tip rupture is wide and short when compared to the narrow and long tip rupture of a small bevel angle needle ($\beta = 30^\circ$). When a tip rupture occurs it is shown that for $\beta = 75^\circ$ coupling of high insertion force and wide and short tip rupture results in more deflection compared to a needle with $\beta = 60^\circ$. A needle with a small bevel angle ($\beta = 30^\circ$) shows that coupling of low insertion force and a long and narrow tip rupture also results in more deflection compared to a needle with $\beta = 60^\circ$.

Increasing the gel elasticity from $E_1 = 8.7$ kPa to $E_3 = 58.1$ kPa results in higher insertion force and needle deflection. There is one exception that does not follow this trend. This exception occurs for the stiffest gel ($E_3 = 58.1$ kPa) and the largest diameter needle ($\phi = 2$ mm). In that case a perpendicular crack occurs during insertion which results in less needle deflection when compared to lower gel elasticities. Four different needle tip shapes were investigated and it was found that a bevel edge needle results in the highest amount of needle deflection due to its asymmetric shape. Insertion force however did not change significantly for all shapes. Different motion profiles were investigated. Results show that adding a 1 Hz sinusoidal rotation to an insertion with a bevel needle decreases the amount of needle deflection but increases the insertion force which could indicate more tissue damage. Increasing the angular velocity decreases the insertion force which could indicate less tissue damage but research in this area is required. A tapping insertion does not result in significant changes in needle deflection but it does increase the insertion force. However this method could still be used in medical procedures since it does result in a decrease of prostate motion as proven by Lagerburg et al. [15].

In this study solid stainless steel wire were used as needles. In future work these will be replaced by actual biopsy needles. Further, it is noted that deflection could only be measured in one plane. The out-of-plane motion was not measured but in the future 3D tracking of the needle will be made possible thus enabling the measurement of 3D needle deflection. Another topic for future work is found in replacing the homogeneous gelatin phantom for an inhomogeneous biological tissue. This tissue would better represent the human body. Further, a study on tissue damage and how the tested parameters have an influence on this is recommended. Results in this study can be used for modeling the needle-tissue interaction. For example, in medical procedures where a needle must be navigated towards a target it is necessary to have path-planning models which incorporate deflection of the needle during insertion. The presented results can help in creating these models.

Chapter 4

Conclusions and Recommendations

This chapter describes conclusions on the graduation assignment and gives recommendations for future work regarding the needle insertion device and future research. To conclude this assignment the assignment description is mentioned again and was:

'Needle and Soft-Tissue Simulant Interactions: Experimental Design and Observations'

In Chapter 2 the design and construction of the 2 DOF needle insertion device is presented and in Chapter 3 a paper is presented which showed results of macroscopic and microscopic observations on needle-tissue insertions.

4.1 Conclusions

A literature research was done on existing needle insertion devices and performed research on the subject of needle-tissue interaction. A list of specifications and requirements was made and based on this list, multiple concepts for a needle insertion device were considered. The concept of a linear stage was chosen and constructed. A great amount of time was spent in creating the software that runs the needle insertion device. The software allows the user to insert a needle with one translational and one rotational degree of freedom into a phantom of varying dimensions. Forces and torques acting on the base of the needle are recorded with an ATI nano17 6DOF force/torque sensor and the insertion can be recorded by either a CCD camera or via ultrasound images. After a proof of principle of the needle insertion device a number of experiments were performed in which observations were made on needle-tissue insertions. The parameters that were subject to research included varying the insertion velocity, the needle diameter, the needle tip bevel angle, needle tip shape, motion profile and gel elasticity. It was shown that with increasing insertion velocity from $v = 5$ mm/s to 300 mm/s the insertion force increases to an asymptote of 6 N and the maximum needle tip deflection decreases to an asymptote of 7.8 mm.

With increasing needle diameter it was shown that the maximum insertion force increases and the maximum needle tip deflection decreases. The decreased amount of tip deflection is due to an increased second moment of inertia of the needle when the diameter is increased.

Increasing the gel elasticity resulted in an increase in maximum insertion force and needle tip deflection. However with the stiffest gel ($E_3 = 58.1$ kPa) and largest needle diameter ($\phi = 2$ mm) it was shown that a perpendicular crack along the insertion direction resulted in less deflection than a needle with $\phi = 1.6$ mm or lower.

An experiment in which the needle bevel angle was varied between $\beta = 8^\circ$ and 82° showed a nonlinear trend for the maximum insertion force and maximum needle tip deflection. The nonlinear trend was explained by microscopic observations of rupture effects of the gelatin at the needle tip. It was shown that needle tip deflection is dependent on a combination of cutting and compression of the gelatin tissue. Several needle tip shapes were used in an experiment to detect the influence of tip shape on exerted forces and needle tip deflection. It was shown that the asymmetric bevel tip resulted in the highest amount of needle tip deflection when compared to a diamond tip, a franseen tip and a conical tip shape. The

maximum insertion force was relatively equal(~ 2.8 N) for all tip shapes indicating that the forces at the tip of a needle are small when compared to the friction forces that act on the needle shaft. The last experiment considered several different motion profiles and it was shown that adding a 1 Hz rotational motion to an insertion decreases the amount of needle tip deflection by ~ 96 %, while the maximum insertion force increases by ~ 12 %. Increasing the angular velocity from 1 Hz to 5 Hz decreases the maximum insertion force by 22 % when compared to the 1 Hz case while the amount of needle tip deflection remained constant. A tapping motion showed no discernible change in needle tip deflection while the maximum insertion force increased by ~ 6 % when compared to a continuous insertion.

The constructed needle insertion device has already proven itself in a number of research publications excluding the presented paper in Chapter 3. The following papers are a direct result from experiments performed with the needle insertion device. They are still under review but have been submitted to a conference.

- 'Mechanics of needle-tissue interaction', R.J. Roesthuis, Y.R.J. van Veen, A. Jahya, and S. Misra, (IROS 2011)
- 'Target motion predictions for pre-operative planning during minimally invasive surgery', J. op den Buijs, Y.R.J. van Veen, C.L. de Korte, and S. Misra, (EMBS 2011)
- 'Effect of skin thickness on target motion during needle insertion into soft tissue phantoms', M. Abayazid, J. op den Buijs, C.L. de Korte, and S. Misra, (IROS 2011)

4.2 Recommendations

During the project a number of issues and/or ideas came up while using the needle insertion device. What follows is a list of recommendations which can be incorporated in the future to improve the usefulness of the device and some recommendations for future research.

4.2.1 Needle Insertion Device

Control of the device

Currently the needle insertion device is controlled with the structure shown in Figure 2.6. This structure has the disadvantage that the overall control is decentralized. For example, the Elmo controllers create the motion profile and perform the motion. Matlab only sends certain parameter values including type of motion, velocity and endposition. During the motion there is no possibility of changing any parameter. The same holds for the F/T sensor and the cameras. They are turned on from matlab but the data can't be used during a motion. It can only be used after the motion has finished. In the future the NID will be used to navigate needles to avoid obstacles during an insertion. This requires that feedback is used to change the path of the needle during an insertion which is currently not possible. It is recommended that the software structure is redesigned in such a way that the control of both motors and all sensors is done in a centralized place and in real-time. A solution could be to make use of the 20-sim 4C Real-Time Toolbox from Controllab Products B.V. 20-sim is a modeling and simulation program originally created in the Control Engineering group of the University of Twente. With the 20-sim 4C real-time toolbox the user can write code to actuate a device and export it to an external target(e.g. the NID). This code actuates the external target in real-time and can use the feedback of sensors directly to change inputs of the motors. Also since 20-sim was created at the Control Engineering group, a great amount of expertise is present with regard to this software. This has the benefit that if problems do arise the expertise is present to solve them quickly. Another possibility is to make use of xPC Target designed by the creators of Matlab. This toolbox works much like 20-sim 4C and can also control an external device in real-time. The benefit of this system is that it is compliant with all other toolboxes of Matlab and as such may be a better option since some of the current software can be reused directly.

Tracking of the needle position

When using a transparent phantom the needle can be seen and recorded by two cameras. A tracking algorithm is then applied to the recorded images to detect the needle. In case of a non-transparent phantom ultrasound images are recorded and another tracking algorithm is applied. However, it has been proven difficult to implement a tracking algorithm that accurately tracks the needle in all the many different phantoms and motion settings that are used in the experiments. A solution can be found in implementing the tracking of the needle position inside the needle itself. This can be done by using Fiber Bragg Grating sensors inside a needle. These sensors consist of optical fibers through which light is transmitted. A short segment of the fiber contains the Fiber Bragg Grating which reflects a particular wavelength of light and transmits all others. This reflected wavelength changes by applying a strain to the optical fiber. By implementing multiple fibers and sensors in a needle it has been shown that these can be used to determine the direction and amount of bending of a needle [26], [27]. The benefit of this type of sensor is that it can be used in any type of phantom, transparent or non-transparent in any lighting condition and/or shape. This eliminates the necessity of a tracking algorithm that works only under certain conditions.

Flexible needles

A goal of the device is to use flexible needles that can be steered around obstacles. However, flexible needles will easily buckle when unsupported. A guidance plug was made to support flexible needles but it was found that this will not support the smallest needles (diameter ≤ 0.8 mm). Therefore it is advised that some modifications are implemented in the current device to support flexible needles along the entire needle length. Some options for this would be to use a telescopic tube like a car antenna through which the needle is passed. During insertion it will collapse inwards and any buckling will be supported by the tube. A drawback of this system is that the force and torque measurements on the base of the needle are highly influenced and will be unusable for accurate measurements. Another option could be that of a support tube which travels along with the insertion of the needle. Any support it is giving to the needle is then a static friction. This will still influence the force and torque measurement but it might be to a lesser degree.

4.2.2 Future research

In Chapter 3 results are shown on macroscopic observations on needle-tissue interaction. The observations looked at forces acting on the base of the needle and deflection of the needle. For future research it can be considered to also look at deflection of the target. Deflection of the needle is of importance on targeting accuracy but deflection of the target during insertion is also important. When the needle is accurately positioned but the target itself has moved then the biopsy or placement of a radioactive seed is still incorrect. In the current research deflection of the target is not considered since the tracking algorithm is not able to track a needle and a target. Another option for future research is implementing the results from the performed experiments in a model. This model could simulate the amount of needle deflection based on the insertion and needle parameters which were tested in Chapter 3. This model can then be used for path planning prior to a needle insertion procedure. The results of the study can also be used in the area of navigating a needle around obstacles. The results of Chapter 3 indicate which kind of needle and with which insertion parameters, result in the most amount of needle deflection. More needle deflection indicates higher maneuverability of the needle and thus better steering capabilities of the needle.

References

- [1] N. Abolhassani, R. Patel, and F. Ayazi. Effects of different insertion methods on reducing needle deflection. In *Proc. Int'l Conf. of the IEEE Engineering in Medicine and Biology Society*, pages 491–494, Lyon, France, August 2007.
- [2] N. Abolhassani, R. Patel, and M. Moallem. Control of soft tissue deformation during robotic needle insertion. *Minimally Invasive Therapy and Allied Technologies*, 15(3):165–176, 2006.
- [3] N. Abolhassani, R. Patel, and M. Moallem. Needle insertion into soft tissue: A survey. *Medical Engineering and Physics*, 29(4):413–431, 2007.
- [4] N. Abolhassani and R. V. Patel. Deflection of a flexible needle during insertion into soft tissue. In *Proc. IEEE Int'l. Conf. Engineering in Medicine and Biology Society (EMBS)*, pages 3858–3861, New York City, USA., August–September 2006.
- [5] R. Alterovitz, K. Goldberg, and A. Okamura. Planning for steerable bevel-tip needle insertion through 2d soft tissue with obstacles. In *Proc. Int'l. Conf. Robotics and Automation (ICRA)*, pages 1640–1645, Barcelona, Spain, April 2005.
- [6] Erik K. Bassett, Alexander H. Slocum, Peter T. Masiakos, Howard I. Pryor II, Omid C. Farokhzad, and Jeffery M. Karp. Design of a mechanical clutch-based needle-insertion device. *Proceedings of the National Academy of Sciences of the United States of America (PNAS)*, 106(14):5540–5545, 2009.
- [7] J. R. Crouch, C. M. Schneider, J. Wainner, and A. M. Okamura. *A velocity-dependent model for needle insertion in soft tissue*, volume 3750 LNCS of *Lecture Notes in Computer Science (including subseries Lecture Notes in Artificial Intelligence and Lecture Notes in Bioinformatics)*. Springer Berlin / Heidelberg, 2005.
- [8] S. P. DiMaio and S. E. Salcudean. Needle insertion modeling and simulation. *IEEE Transactions on Robotics and Automation*, 19(5):864–875, 2003.
- [9] H. Elhawary, Z.T.H. Tse, M. Rea, A. Zivanovic, B. Davies, C. Besant, N. de Souza, D. McRobbie, I. Young, and M. Lamperth. Robotic system for transrectal biopsy of the prostate: Real-time guidance under mri. *IEEE Engineering in Medicine and Biology Magazine*, 29(2):78–86, march–april 2010.
- [10] J. J. Fütterer, S. Misra, and K. J. Macura. Mri of the prostate: potential role of robots. *Imaging in Medicine*, 2(5):583–592, 2010.
- [11] D. Glozman and M. Shoham. Image-guided robotic flexible needle steering. *IEEE Transactions on Robotics*, 23(3):459–467, 2007.
- [12] KWF Kankerbestrijding. Kanker in nederland, trends, prognoses en implicaties voor zorgvraag, October 2004.
- [13] Hiroyuki Kataoka, Toshikatsu Washio, Kiyoyuki Chinzei, Kazuyuki Mizuhara, Christina Simone, and Allison M. Okamura. Measurement of the tip and friction force acting on a needle during penetration. In *Proc. of the 5th Int'l. Conf. on Medical Image Computing and Computer-Assisted Intervention-Part I, MICCAI '02*, pages 216–223, London, UK, September 2002. Springer-Verlag.

-
- [14] T. A. Krouskop, T. M. Wheeler, F. Kallel, B. S. Garra, and T. Hall. Elastic moduli of breast and prostate tissues under compression. *Ultrasonic imaging*, 20(4):260–274, 1998.
- [15] V. Lagerburg, M. A. Moerland, M. K. Konings, R. E. Van De Vosse, J. J. W. Lagendijk, and J. J. Battermann. Development of a tapping device: A new needle insertion method for prostate brachytherapy. *Physics in Medicine and Biology*, 51(4):891–902, 2006.
- [16] V. Lagerburg, M. A. Moerland, M. van Vulpen, and J. J. W. Lagendijk. A new robotic needle insertion method to minimise attendant prostate motion. *Radiotherapy and Oncology*, 80(1):73–77, 2006.
- [17] M. Mahvash and P.E. Dupont. Mechanics of dynamic needle insertion into a biological material. *IEEE Transactions on biomedical engineering*, 57(4):934–943, 2010.
- [18] M. A. Meltsner, N. J. Ferrier, and B. R. Thomadsen. Observations on rotating needle insertions using a brachytherapy robot. *Physics in Medicine and Biology*, 52(19):6027–6037, 2007.
- [19] S. Misra, K. B. Reed, A. S. Douglas, K. T. Ramesh, and A. M. Okamura. Needle-tissue interaction forces for bevel-tip steerable needles. In *Proc. IEEE Int'l. Conf. Engineering in Medicine and Biology Society (EMBS)*, pages 224–231, Scottsdale, AZ, USA, August 2008.
- [20] S. Misra, K. B. Reed, K. T. Ramesh, and A. M. Okamura. Observations of needle-tissue interactions. *IEEE Engineering in Medicine and Biology Society*, pages 262–265, 2009.
- [21] S. Misra, K. B. Reed, B. W. Schafer, K. T. Ramesh, and A.M. Okamura. Observations and models for needle-tissue interactions. In *Proc. IEEE Int'l. Conf. Robotics and Automation(ICRA)*, pages 2687–2692, Kobe, Japan, May 2009.
- [22] S. Misra, K. B. Reed, B. W. Schafer, K. T. Ramesh, and A.M. Okamura. Mechanics of flexible needles robotically steered through soft tissue. *Int'l. J. Robotics Research*, 29(13):1640–1660, 2010.
- [23] A. M. Okamura, C. Simone, and M. D. O’Leary. Force modeling for needle insertion into soft tissue. *IEEE Transactions on Biomedical Engineering*, 51(10):1707–1716, 2004.
- [24] M. D. O’Leary, C. Simone, T. Washio, K. Yoshinaka, and A. M. Okamura. Robotic needle insertion: Effects of friction and needle geometry. In *Proceedings of the 2003 IEEE International Conference on Robotics and Automation*, volume 2, pages 1774–1780, Taiwan, Taipei,, September 2003.
- [25] Y.L. Park, K. Chau, R.J. Black, and M. R. Cutkosky. Force sensing robot fingers using embedded fiber bragg grating sensors and shape deposition manufacturing. In *Proc. IEEE Int'l Conf. on Robotics and Automation (ICRA)*, pages 1510–1516, April 2007.
- [26] Y.L. Park, S. Elayaperumal, B.L. Daniel, E. Kaye, K.B. Pauly, R.J. Black, and M.R. Cutkosky. Mri-compatible haptics: Feasibility of using optical fiber bragg grating strain-sensors to detect deflection of needles in an mri environment. Int’l Society for Magnetic Resonance in Medicine (ISMRM) 16th Scientific Meeting and Exhibition, May 2008.
- [27] Y.L. Park, S. Elayaperumal, S. Ryu, B. Daniel, R.J. Black, B. Moslehi, and M. R. Cutkosky. Mri-compatible haptics: Strain sensing for real-time estimation of three dimensional needle deflection in mri environments. Int’l Society for Magnetic Resonance in Medicine (ISMRM) 17th Scientific Meeting and Exhibition, April 2009.
- [28] T. K. Podder, D. P. Clark, D. Fuller, J. Sherman, W. S. Ng, L. Liao, D. J. Rubens, J. G. Strang, E. M. Messing, Y. D. Zhang, and Y. Yu. Effects of velocity modulation during surgical needle insertion. In *Proc. IEEE Int'l. Conf. Engineering in Medicine and Biology Society (EMBS)*, pages 5766–5770, Shanghai, China, September 2005.

-
- [29] K. B. Reed, V. Kallem, R. Alterovitz, K. Goldberg, A. M. Okamura, and N. J. Cowan. Integrated planning and image-guided control for planar needle steering. In *Proc. of the 2nd Biennial IEEE/RAS-EMBS Int'l Conf. on Biomedical Robotics and Biomechatronics (BioRob)*, pages 819 – 824, Scottsdale, AZ, USA, 2008.
- [30] K. B. Reed, A. M. Okamura, and N. J. Cowan. Modeling and control of needles with torsional friction. *IEEE Transactions on Biomedical Engineering*, 56(12):2905 – 2916, 2009.
- [31] Siemens magnetom - technical specifications. www.medical.siemens.com, 2011.
- [32] American Cancer Society. Cancer facts and figures 2010, 2010.
- [33] M. J. Steggerda, H. G. van der Poel, and L. M. F. Moonen. Minimizing the number of implantation needles for prostate 125i brachytherapy: An investigation of possibilities and implications. *Brachytherapy*, 9(4):319–327, 2010.
- [34] R. J. Webster III, J. Memisevic, and A. M. Okamura. Design considerations for robotic needle steering. In *Proc. IEEE Int'l Conf. on Robotics and Automation (ICRA)*, pages 3588 – 3594, Barcelona, Spain, April 2005.
- [35] R.J. Webster III, J.S. Kim, N.J. Cowan, G.S. Chirikjian, and A.M. Okamura. Nonholonomic modeling of needle steering. *Int'l. J. Robotics Research*, 25(5-6):509–525, 2006.
- [36] C. H. Xiao and H.C. Yung. Corner detector based on global and local curvature properties. *Optical Engineering*, 47(5):1–12, 2008.

Appendices

Appendix A

Motor Calculations

Translation of the needle Goal: To derive what the motor and gearhead characteristics should be to actuate the linear stage. The maximum required torque and the RMS torque for a worst case motion profile are calculated. With the calculated torques a gearhead and motor are chosen. In Figure A an Ideal Physical Model of the stage translator is shown. These are divided into three Free Body Diagrams (Figures A.3, A.4 and A.5).

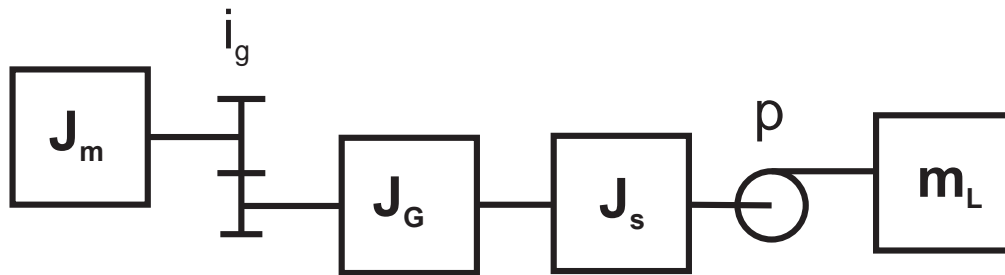


Figure A.1: IPM of the motor, gearhead, spindle and load

parameters In Table A.1 a number of parameters are shown which will be used in the calculations. These values are either known or assumed from the specifications and requirements.

Maximum mass of the load	m_L	=	1	kg
Maximum stroke of the carriage	s	=	150	mm
Maximum velocity	v	=	300	mm/s
Maximum acceleration of the carriage	a_{\max}	=	10	m/s^2
Spindle lead	p	=	10	mm

Table A.1: Parameters

Assumptions

- Rigid spindle ($\theta_g - \theta_s = 0$ torsion of the spindle is zero and also the spring stiffness between the spindle and load is infinite ($p \cdot \theta_s = x$))

Desired motion Required torques of the motor and gearhead are dependant on the motion profile of the carriage. In Figure A.2, a worst case scenario for the motion profile is shown. This motion profile will be used to calculate the required torques for the motor and gearhead. It consists of a motion in which the carriage travels 150mm with a velocity of 300 mm/s. This velocity is reached with an acceleration of 10 m/s^2

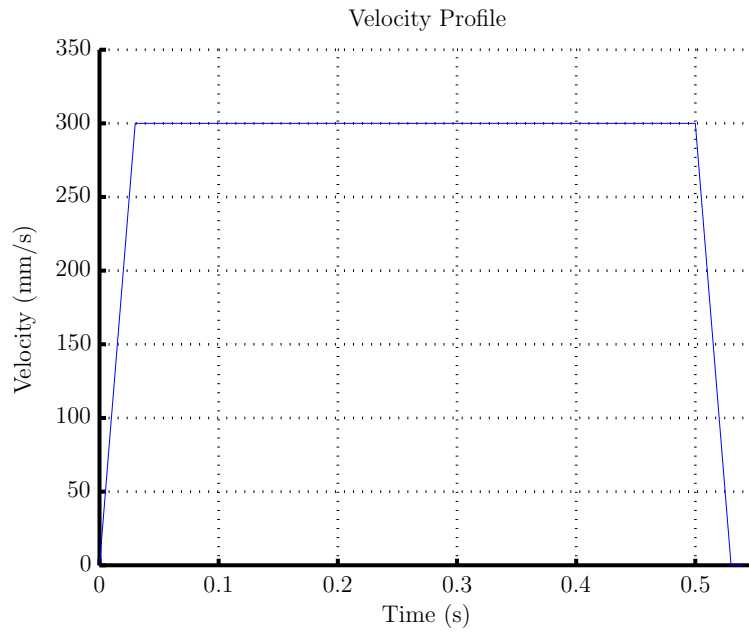


Figure A.2: Velocity profile

The following time values are used:

acceleration	time_{acc}	=	0.03	s
motion	$\text{time}_{\text{motion}}$	=	0.47	s
braking	$\text{time}_{\text{brake}}$	=	0.03	s
total motion time	time_{tot}	=	0.53	s

Table A.2: Motion profile time parameters

Free Body Diagram - Load (carriage + needle attachment) In Figure A.3, a free body diagram of the load is shown. From Equation A.1 we can calculate the desired load force.

$$\sum F = m \cdot a \Rightarrow$$

$$F_L = m_L \cdot a_{max} \quad (A.1)$$

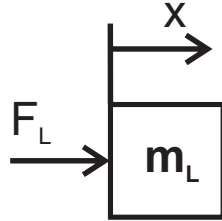


Figure A.3: Free Body Diagram of the Load

Free Body Diagram - Gearhead + Spindle Parameters for the calculation are shown in Table A.3. There is no prior knowledge on the moment of inertia of the gearhead so this is assumed to be zero. It is also assumed due to lack of information that the starting torque of the linear stage equals the dynamic friction.

Moment of inertia of gearhead	J_g	=	0	Nm
Moment of inertia of the spindle	J_s	=	$6.24 \cdot 10^{-6}$	kgm ²
Acceleration of gearhead	$\ddot{\theta}_g$	=	$a_{max} \left(\frac{2\pi}{p} \right)$	rad/s ²
Starting torque	M_f	=	0.04	Nm
Load torque	M_L	=	$F_L \frac{p}{2\pi}$	Nm

Table A.3: Parameters

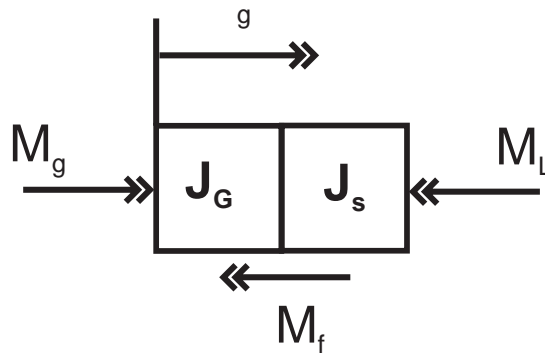


Figure A.4: Free Body Diagram Spindle + Gearhead

Transmission ratio	$i_g =$	4.4:1	
Transmission ratio absolute		57/13	
Max. continuous torque		0.5	Nm
Intermittent permissible torque at gear output		0.8	Nm
Max. efficiency	$\eta =$	84	%
Mass inertia		0.6	gcm ²
Max. recommended input speed		<8000	rpm

Table A.4: Parameters of Maxon Gearhead GP26B

The maximum intermittent torque (M_g) that the gearhead should deliver is calculated as follows:
 $\sum M = J \cdot \alpha \Rightarrow (J_g + J_s) \cdot \ddot{\theta}_g = M_g - M_L - M_f \Rightarrow$

$$M_g = (J_g + J_s) \cdot \ddot{\theta}_g + M_L + M_f \quad (\text{A.2})$$

Besides that there is also the max-continuous-torque (M_{gRMS}) which is calculated as follows

$$M_{gRMS} = \sqrt{\frac{1}{t_{tot}} \cdot (t_{acc} \cdot M_g^2 + t_{motion} \cdot M_f^2 + t_{brake} \cdot (M_g - 2M_f)^2)} \quad (\text{A.3})$$

From this the following values are calculated $M_{gRMS} = 43.7$ mNm and $M_g = 95.1$ mNm. With these values for M_g and M_{gRMS} a gearhead is chosen. The Maxon GP26B with a transmission ratio of 4.4:1 was chosen. The specifications of the gearhead are shown in Table A.4.

As can be seen the desired intermittent torque at the gearhead output is a little bit higher than the gearhead may deliver but the manufacturer stated that this difference was not a problem. Further, the moment of inertia of the gearhead is one hundred times smaller than the moment of inertia of the spindle and thus the assumption of $J_g = 0$ was justified. With this gearhead the motor requirements are calculated.

Free Body Diagram - Motor In Figure A.5 a free body diagram of the motor is shown. In Table A.5 some parameters are shown which are used in the following calculations. It is assumed that the moment of inertia of the motor is zero due to lack of knowledge. It will later be shown that this assumption could be made.

The maximum intermittent torque is calculated as follows: $\sum M = J \cdot \alpha \Rightarrow M_m - M_n = J_m \cdot \ddot{\theta}_m \Rightarrow$

$$M_m = J_m \cdot \ddot{\theta}_m + M_n \quad (\text{A.4})$$

Again there is also the maximum continuous torque which is derived from the maximum continuous torque of the gearhead as follows:

$$M_{mRMS} = \frac{M_{gRMS}}{i_g \cdot \eta} \quad (\text{A.5})$$

From Equation A.4 it is calculated that the max intermittent torque that the motor should deliver, equals $M_m = 25.7$ mNm. From Equation A.5 we get that $M_{mRMS} = 11.8$ mNm. With these values a motor can be chosen. The Maxon RE25 motor was chosen. The rotor inertia of this motor equals $J_m = 1.07 \cdot 10^{-6}$ kgm². When we multiply this with the desired motor axis acceleration ($\ddot{\theta}_m$) we get a torque of $J_m \cdot \ddot{\theta}_m = 29.6$ mNm. Combined with the previously calculated intermittent torque of $M_m = 25.7$ mNm we get that the total maximum intermittent torque acting on the motor equals $M_m = 55.3$ mNm which is lower than the stall torque of 257 mNm so the assumption of $J_m = 0$ mNm could be made.

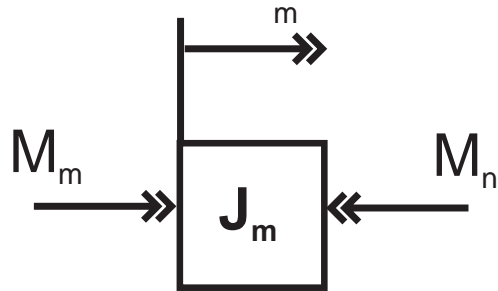


Figure A.5: Free Body Diagram Motor

Moment of inertia of the motor	J_m	$=$	0	Nm
Acceleration of the motor	$\ddot{\theta}_m$	$=$	$\ddot{\theta}_g \cdot i_g$	$\frac{\text{rad}}{\text{s}^2}$
Torque acting on the motor	M_n	$=$	$\frac{M_g}{\eta \cdot i_g}$	Nm

Table A.5: Parameters

Assigned power rating	20	W
Nominal voltage	24	V
No load speed	9550	rpm
Stall torque	257	mNm
Max. continuous torque	26.7	mNm
Speed / torque gradient	38.1	$\frac{\text{rpm}}{\text{mNm}}$
No load current	36.9	mA
Starting current	11	A
max. continuous current	1.17	A
Max. efficiency	86	%
Rotor inertia	10.7	gcm ²
Max. permissible speed	14000	rpm

Table A.6: Maxon RE25 motor parameters

Rotation of the needle

Goal: To derive what the motor characteristics should be to rotate the needle and F/T sensor. The maximum required torque and RMS torque for a worst case motion profile are calculated. With the results a motor is chosen. In Figure A.6 an Ideal Physical Model is shown. It is assumed that the load is rigidly attached to the motor and no gearhead is incorporated.



Figure A.6: Ideal Physical Model of rotation of the needle

Desired motion Required torques of the motor and gearhead are dependant on the motion profile of the needle. The worst case position profile is shown in Figure A.7. It consists of a 5Hz motion with an angular amplitude of 90° , or in other words $\frac{\pi}{2}$ radians. This position profile is shown in Equation A.6. The acceleration profile can be obtained by differentiating the position profile twice and from this the maximum acceleration is be obtained.

$$\theta_m = 90 \cdot \sin(2\pi 5t) \quad (\text{A.6})$$

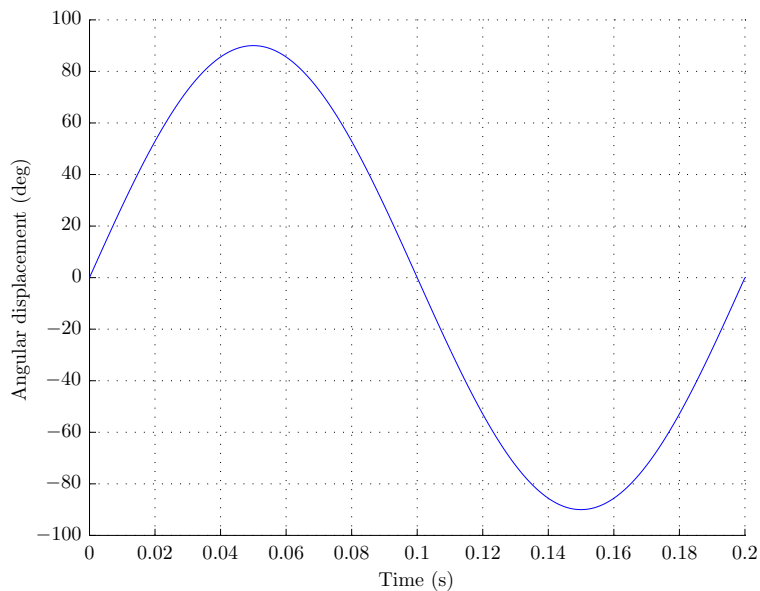


Figure A.7: Position profile - frequency 5 Hz - angular displacement 90 degrees

Free Body Diagram: Motor In Figure A.8, a free body diagram of the load is shown. In Table A.7 the used parameters of the calculation are shown. The inertia of the load was obtained with Solidworks since the geometry was too complex to use standard inertia formulas. It was assumed that all parts were made from stainless steel with a density of 7930 kgm^2 . On top of this a safetyfactor of 2 is applied to

the inertia to account for the inaccuracy that exists due to the excentric F/T sensor cable of which very little is known in terms of data like, weight, stiffness and length. It is also assumed that the inertia of the motor is zero due to lack of knowledge. The maximum frictional torque is assumed to be 3 mNm based on results obtained by Podder et al. [28].

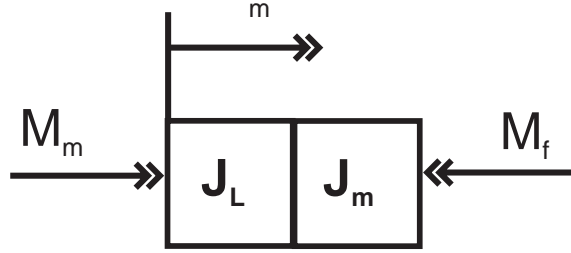


Figure A.8: Free Body Diagram Motor Needle Rotation

Inertia of the motor	J_m	=	0	kgm ²
Maximum inertia of the load	J_L	=	$5.5e^{-6}$	kgm ²
Maximum acceleration of the motor	$\ddot{\theta}_m$	=	$\frac{\pi}{2}(2\pi 5)^2$	$\frac{\text{rad}}{\text{s}^2}$
Maximum frictional torque	M_f	=	3	mNm

Table A.7: Calculation Parameters

Calculation of necessary torque:

The maximum intermittent motor torque is calculated as follows:

$$\sum M = J \cdot \ddot{\theta} \Rightarrow M_m - M_f = J_L \cdot \ddot{\theta}_m \Rightarrow$$

$$M_m = J_L \cdot \ddot{\theta}_m + M_f \quad (\text{A.7})$$

The motor continuous torque is calculated as follows.

$$M_{mRMS} = \sqrt{\frac{1}{t_2 - t_1} \int_{t_2}^{t_1} M_m(t)^2 dt} \quad (\text{A.8})$$

in which

$$\begin{aligned} M_m(t) &= J_L \cdot \ddot{\theta}_m(t) + M_f \\ \ddot{\theta}_m(t) &= -\frac{\pi}{2} \cdot (2\pi 5)^2 \sin(2\pi 5t) \\ t_1 &= 0 \\ t_2 &= 0.2 \end{aligned}$$

t_1 and t_2 were chosen so that at least one period of the sinusoidal position profile was performed. From this we get $M_{mRMS} = 6.7$ mNm. With the two values the brushless maxon ECOMax22 motor was chosen. Due to the device mostly performing rotations of 180° it was specifically chosen to be a brushless motor. The repeated change of rotation direction would increase the amount of wear and tear on the brushes. In Table A.8 the important parameters of this motor are shown.

Assigned power rating	12	W
Nominal voltage	24	V
No load speed	12100	rpm
Stall torque	35.1	mNm
Max. continuous torque	11	mNm
Speed / torque gradient	18.1	rpm/mNm
No load current	72.7	mA
Starting current	1.94	A
max. continuous current	0.659	A
Max. efficiency	66	%
Rotor inertia	2.25	gcm ²
Max. permissible speed	18000	rpm

Table A.8: Maxon ECTMax22 motor parameters

Appendix B

Design Concepts

Besides the chosen linear stage concept, other concepts were considered. These were not chosen for a number of reasons and will be discussed in the following appendix. These concepts are a linear motor concept, a robotic arm concept and a friction drive concept.

B.1 Linear motor

This concept consists of a linear motor to actuate the translational degree of freedom as shown in Figure B.1. A linear guide would then be used to attach a second motor which could rotate the needle. This concept is capable of reaching insertion velocities of up to 4 m/s and accelerations of up to 350 m/s² according to the manufacturer of the linear motor (LinMot, Inc. Elkhorn, USA). The concept was rejected for a number of reasons the first being that the price was higher when compared to the linear stage concept. The second argument comes from difficulties in communication with the LinMot company. Numerous mails and phonecalls were not answered and thus little information could be obtained on the system. However just before the final concept selection, the LinMot company responded. The final concept selection was put on hold to investigate whether this system could work but eventually it was decided this concept would not be investigated further due to time constraints.



Figure B.1: Linear Motor with guide from the LinMot company.

B.2 Robotic arm

This concept consists of two motorized arms which can be individually actuated. At the end of the arms a rotary motor could be implemented to rotate the needle about its longitudinal axis. An idea of the setup can be seen in Figure B.2. The setup would have three actuated degrees of freedom being one translational and two rotational. The concept was rejected because of the added complexity of the design with regard to performing the translational motion. Both motors have to rotate at exactly the same velocity to achieve a straight insertion of the needle. Besides this it was decided that the third degree of freedom was not necessary.

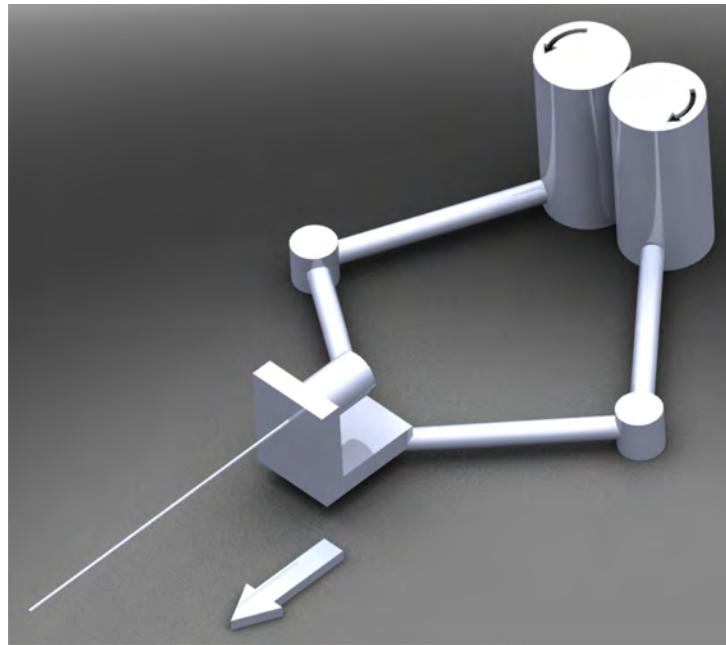


Figure B.2: Robotic arm concept. Rotating the two motors results in a translation of the needle as shown by the arrows

B.3 Friction drive concept

See Fig. B.3 for an example of this concept. The needle is clutched between two rollers which are actuated by a motor. When these rollers rotate, the needle is inserted due to the friction between the roller and the needle. When another motor is added or the rollers are mounted in an angle with respect to one another the needle could also be rotated around the axial direction. The concept was not chosen based on the fact that this concept is prone to slippage between the needle and rollers [34]. Slippage could occur and then there would be no way of determining how far the needle has entered the phantom with only the encoder feedback from the rollers. The benefit of this system would be that due to the short distance between the phantom and the needle-roller contact point, buckling of the needle would most likely not occur and thus it would be suitable for flexible needles.

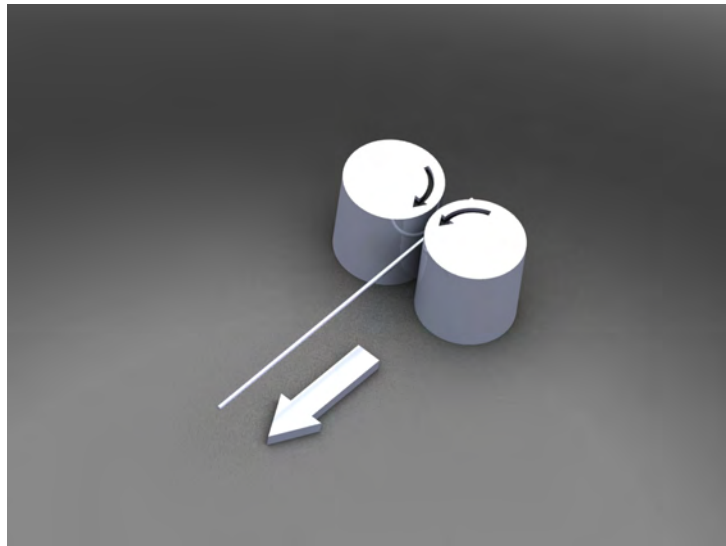


Figure B.3: Friction drive concept. Rotating the two rollers which are pressed against the needle results in a translation of the needle as shown by the arrows

